Creation of interfaces in composite/hybrid nanostructured materials using supercritical fluids

Oana Pascu, Samuel Marre, Cyril Aymonier

Review

Oana Pascu, Samuel Marre and Cyril Aymonier*

Creation of interfaces in composite/hybrid nanostructured materials using supercritical fluids

DOI 10.1515/ntrev-2015-0009
Received February 18, 2015; accepted July 17, 2015; previously published online October 24, 2015

Abstract: By structuring matter at the nano level using highly versatile nanotechnology approaches and apparatus, multifunctionalities with manifestation of enhanced and/or novel useful properties could be attained. The challenges in nanoengineering are the ability to tune the nano-object characteristics (size, distribution, composition, and surface chemistry) and to have a good control on the possible synergy created at the interfaces, especially in the case of complex multifunctional materials. Surface nanoengineering goes hand in hand with the creation of interfaces between nano-objects – either inorganic or hybrid ones – and a closer look in this direction is essential. The present review aims at presenting the possibilities of surface nanoengineering by versatile approaches, namely supercritical fluids processes. Two main routes of nanostructuration, each containing three concepts, will be discussed: supercritical fluid chemical deposition performed in batch mode and continuous supercritical fluid synthesis. Both approaches can be used to access interesting materials with desired properties, with the choice of process depending on what the readers are pursuing.

Keywords: interfaces; nanomaterials; supercritical fluid processes.

***Corresponding author: Cyril Aymonier,** CNRS, University of Bordeaux, ICMCB, UPR 9048, F-33600 Pessac, France, e-mail: cyril.aymonier@icmcb.cnrs.fr
Oana Pascu and Samuel Marre: CNRS, University of Bordeaux, ICMCB, UPR 9048, F-33600 Pessac, France

1 Introduction

1.1 Surface nanostructuration with two types of interfaces, inorganic-inorganic and organic-inorganic

Rational design and development of nanostructured materials, when at least one of the components is <100 nm, with unique properties and high performances, are hot topics for both scientific [1–7] and industrial communities [8–17]. By combining two or more inorganic and/or organic components with different individual properties, a plethora of multifunctional materials based on inorganic/hybrid nanostructures are obtained [1, 2, 6, 8, 9, 11, 12, 16]. It is worth stressing that only by becoming part of a hybrid combination, exotic in many ways, could manifestation of enhanced and/or novel useful properties be attained [1]. This multifunctionality can be achieved by structuring matter at the nano level using highly versatile nanotechnology approaches and appliances [2]. In the nanostructuration field, the challenges are (i) the nanosize and narrow size distributions of nanocomponents, (ii) precise and controlled morphologies, (iii) composition and functionality, (iv) a good knowledge of the phenomena at the nanointerfaces, and (v) the physical and chemical compatibility of individual components, all these being in close relationship with material properties. Moreover, it has to be highlighted that the properties of inorganic/hybrid nanostructures are not only the results of summing the individual properties but could also arise from a possible synergy created at the interfaces [1]. The considerable struggle in recent years, summarized in various reviews [1–17], stands in a better control and manipulation of materials' structure-properties correlation, opening novel applications opportunities, e.g. as mechanical metamaterials [13], conductive nanomaterials [14], energy storage [12], neural [17], or cell-material smart interfaces [6].

Materials that have been the subject of intense research could be listed in two major categories, namely inorganic

and hybrid nanostructures, implying the existence of interfaces. Metal and metal oxide semiconductors can be either shaped as conformal nano-thin films deposited onto various inorganic solid surfaces or in the form of nanoparticles (NPs), uniformly distributed or incorporated into non-porous inorganic supports, giving rise to a fully inorganic nanostructuration. In the case of hybrid inorganic-organic composition, the organic moieties can be either the framework (e.g. NPs incorporated into polymer matrices) or placed at the nano-object surface (e.g. inorganic NPs coated with organic shells). It has been found [1, 7, 18–22] that the crucial role of surface chemistry and interface within these systems is influencing the placing of nano-objects with precise control of their morphology, composition, and functions. For example, in the case of supported metallic NPs, depending on the inorganic support type and metal type, not only different NP morphologies and organization could be achieved [18] but also a chemical coupling between metal NPs and the active support can be made [19]. We also demonstrated that the reaction media could behave as surface modifiers [21, 22] or sources of non-metal incorporation into the metal lattice [20]. With these, we emphasize the importance of the coupling between the elected synthesis methods and the surface/interface chemistry, which will have a direct influence on the physico-chemical properties of the final hybrid material.

The nanostructured material's properties and applications dictate the direction of its fabrication and the necessity to design and optimize new synthetic approaches. Among the multitude of applied fabrication technologies already mentioned in recent reviews [1–17, 23–26], the supercritical fluid (SCF) technology, as a versatile approach for designing advanced nanostructured materials, is worthwhile to be considered. In the following, we are making a short introduction to the SCF technology. Strong attention is paid to the physico-chemical properties of SCFs and to the technology's principle as an alternative synthesis method.

1.2 SCF routes

SCF approaches have shown considerable development during the last two decades, being considered as convenient alternatives to the conventional synthesis methods.

1.2.1 What makes SCFs so special [3, 23–28]?

First of all, a SCF is a single-phase domain (Figure 1A), with no phase boundary between the gas and liquid phases, which properties can be continuously adjusted from liquid to gas and vice versa. This continuity in thermophysical properties (density, viscosity, and diffusivity) induces "hybrid properties" of both liquid and gas, changeable with small variations of temperature or pressure. The properties of SCFs are unusual and are characterized by liquid-like densities, gas-like viscosities, and (much) higher diffusivities than in liquids (Figure 1C). Secondly, above the fluids' critical points (Figure 1A), there is a quasi-zero

A

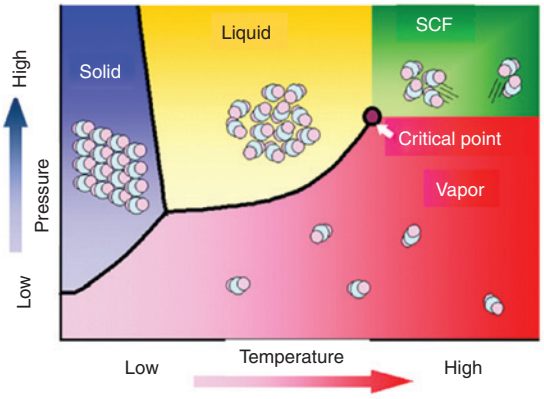

B

Fluid	T_c (°C)	P_c (MPa)
CO_2	31	7.38
H_2O	374	22.1
MeOH	240	7.95
EtOH	243	6.39
CO_2:EtOH*	65	9.9
IPA	235.6	5.37

*EtOH molar fraction=0.05; EtOH-ethanol; MeOH-methanol; IPA-isopropanol;

C

Fluid properties	Vapor	SCF	Liquid
Density (g/cm^3)	0.6–2×10^{-3}	0.2–0.9	0.6–1.6
Diffusivity (m^2/s)	1–4×10^{-5}	2–7×10^{-8}	10^{-9}
Viscosity (Pa/s)	1–3×10^{-5}	1–9×10^{-5}	10^{-3}

Figure 1: Pressure-temperature phase diagram (A) with the critical data of some fluids [NIST database] (B) and the comparison of typical properties of vapor, supercritical fluid and liquid (C) [24].

surface tension, this being an important feature for surface and interface chemistry. Thirdly, the solvent plays a critical role in the preparation of nanomaterials in SCFs, strongly influencing the nature of the final material. Therefore, material syntheses at supercritical conditions can be seen as liquid-phase approaches in environments that behave like gases. This means that these syntheses can process all types of solution-based reactions with a wide range of available surfactants/precursors systems allowing accessing enhanced control over the materials' size, shape, and surface functionalities. Additionally, SCF processes are not limited by vapor pressure considerations, thus enlarging the space for synthesis in the whole phase diagram. As a consequence, this gives access to a fine control over reaction kinetics. Meanwhile, SCFs provide environments for nucleation and growth of NPs, close to the ones encountered in gas-phase synthesis approaches at the origin of the formation of highly crystalline materials.

The most employed solvents are CO_2 and H_2O; however, when designing the material synthetic path, they could be the combination of two or more fluids, the mixture thus having different properties, which can be clearly seen in the modification of critical pressures and temperatures, specific to defined compositions (Figure 1B). These thermodynamics – essential to design processes – can be obtained through the use of high-pressure cells, although we recently demonstrated much faster microfluidic approaches for investigating these multicomponent systems' thermodynamics under pressure and temperature [29, 30]. The solubility of the precursors being dependent on the solvent's density could be controlled by slight changes in the reaction's pressure and temperature, or by the addition of co-solvent(s). For instance, the addition of alcohol in CO_2 increases the solubility of polar reactants, or the addition of alcohol to water allows decreasing the critical coordinates of the fluid system while boosting crystallization [3, 26, 27]. An increased mass and heat transfer, resulting in faster kinetics, are also useful ingredients to prepare functional materials [28].

A summarized view of the different concepts allowing building inorganic or hybrid nanostructured materials using SCF approaches can be splitted into two main paths labeled (i) SFCD (supercritical fluid chemical deposition – in batch mode) and (ii) CSFS (continuous supercritical fluid synthesis), each path including three concepts, namely cold wall reactor, thermodynamic and kinetic controls (for SFCD), and the synthesis of naked NPs or hybrid organic/inorganic NPs through *in situ* or *ex situ* functionalization of nanostructures, and co-flow reactor for nanostructuring (for CSFS), as shown in Figure 2. The nanostructuration is obtained through the manipulation of molecular precursor (metal-organic or inorganic salts) reactivity with control

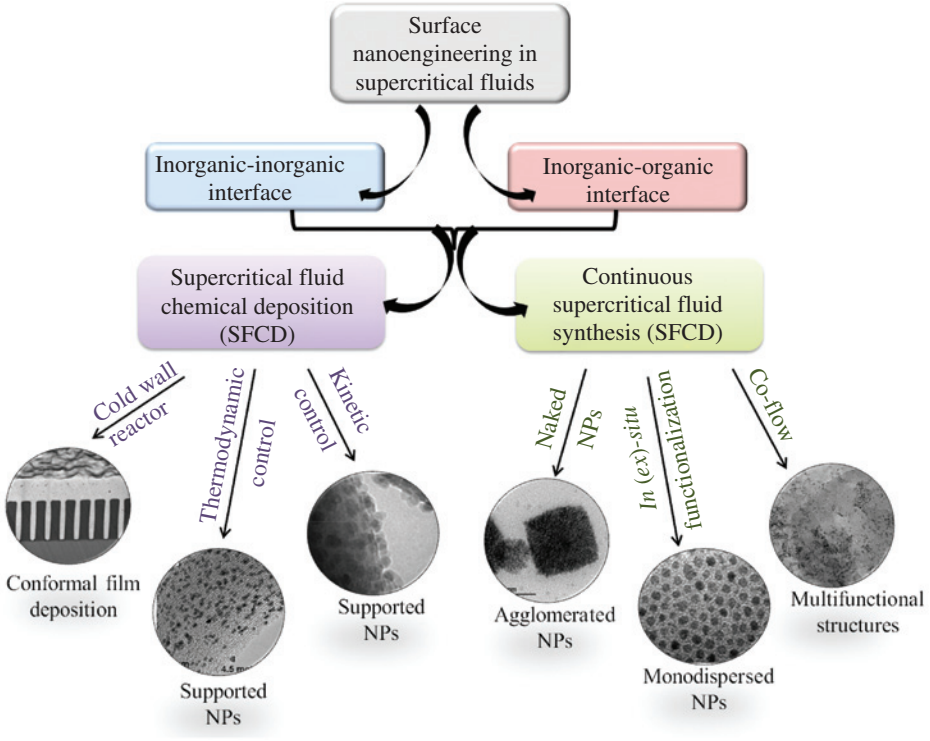

Figure 2: Sketch of the different concepts used in supercritical fluids technologies to build advanced inorganic or hybrid nanostructures.

over nucleation, growth, and aggregation processes [1, 3]. The reaction can be controlled by tuning the physical and chemical parameters of the supercritical media.

SFCD allows material surface and volume nanoengineering [23, 25, 31, 32], being developed as an alternative to classical chemical vapor deposition (CVD) in order to satisfy the current nanostructuring high demands, such as conformal coverage of complex topographies, entire filling of narrow high aspect ratio features, low process temperatures, reduction of wastes from current processing technologies, etc. [31]. The pioneer in using SFCD as a new approach for the preparation of nanosized thin metal films, involving the chemical reduction of soluble metallic compounds in supercritical carbon dioxide at low temperature, was the Watkins group [33]. They developed the cold wall reactor concept [33, 34], allowing the excellent conformal deposition of thin films on patterned substrates, thanks to a heterogeneous growth over the heated substrates, being moreover free from any ligand (organic) contamination. Moving from the cold wall to the hot wall, stirred batch reactor allows depositing metal NPs onto the surfaces of porous solid supports or within polymers, resulting from homogeneous nucleation in the reactive media. Different groups (Erkey et al., Türk et al., Cabanas et al., and others) developed the thermodynamically controlled surface nanostructuration [23–25, 35, 36], while our group introduced the kinetically controlled surface nanostructuration, as fast and versatile concepts of SFCD [32, 37]. A brief description of each concept followed by relevant examples will be presented in Section 2.1.

The continuous synthesis of NPs (CSFS) from molecular precursors in supercritical solvents (water and/or organic) has reached high finesse for the control of structural, morphological, and textural features (Figure 2). By optimizing several experimental parameters (precursor type and concentration, presence or absence of surfactant(s), reaction temperatures, flow rates, tubing type, residence time, etc.), efficient nanomaterials for various applications (catalysis, electronics, optics, etc.) can be prepared. Many groups (Adschiri et al., Iversen et al., Lester et al., Türk et al., our group, and others) have brought important contributions to the field, developing continuous synthesis approaches for hybrid NPs with a control over nucleation and growth of the NPs. The synthesis of single nanocrystals (NCs) of a variety of naked or hybrid metal and metal oxide in supercritical water was developed by the Adschiri group [38], reporting the versatility of hydrothermal synthesis not only for controlling the oxidizing and reducing atmosphere, but also for the *in situ* NC surface modification with organic ligands, making them dispersible in organic solvents. On the other hand, our group proposed to separate and control the nucleation/growth from the functionalization steps either by adding the stabilizing agent *ex situ* or by introducing the co-flow system, thus bringing a complementary contribution to the scientific community. Some of the most relevant results are presented in Section 2.2.

The versatility of SCF technologies stands not only in the preparation of effective functional materials with complicated architectures [3, 23–27], less accessible by conventional methods, using batch mode (SFCD), but also in the capability to achieve one-pot synthesis of multifunctional nanostructures in a continuous way (CSFS). While the batch mode allows accessing nanostructures with complicated architectures of high quality and good properties, the fast continuous mode (residence time from a few seconds to a few minutes) allows synthesizing high-quality nanomaterials (well-crystallized, narrow size distribution, pure-phase stoichiometry, etc.) [26, 39–41].

2 Nanoengineering approaches

2.1 Batch-mode SFCD

As already mentioned, SFCD is a significant alternative to classical CVD in designing inorganic or hybrid nanostructured materials. The nano-objects could be either nanofilms or NPs, conformally deposited onto a support. The SFCD working principle is as follows: dissolution of metal precursor in SCFs followed by its chemical reduction. Owing to the liquid-like densities of SCFs, the dissolved metallic precursor concentration can be almost three times higher than in CVD, leading to an increased mass transfer, thus promoting a high conformal coverage [33, 34]. Additionally, the gas-like properties – low viscosities, high diffusivities, and quasi-zero surface tensions – promote an effective nanostructuration of complicated architectures and confined geometries.

The first reported SCF chemical deposition (by Watkins et al.) consisted in the preparation of pure platinum metal film onto an inorganic (silicon wafer and porous alumina) or polymer substrate at low temperature (80°C) [33]. The metal precursor [organometallic-dimethyl-(cyclooctadiene) platinum(II) ($CODPtMe_2$)] transport occurs in solution (sc-CO_2 media), and the reduction in the presence of H_2 (hydrogenolysis) occurs at the solution-solid interface. The pure metal Pt has been deposited on Si wafer in the form of a continuous 1.3 μm thick film and made of 80–100 nm Pt NCs (Figure 3A), while clusters of 30 nm were deposited inside the alumina pores (~200 nm)

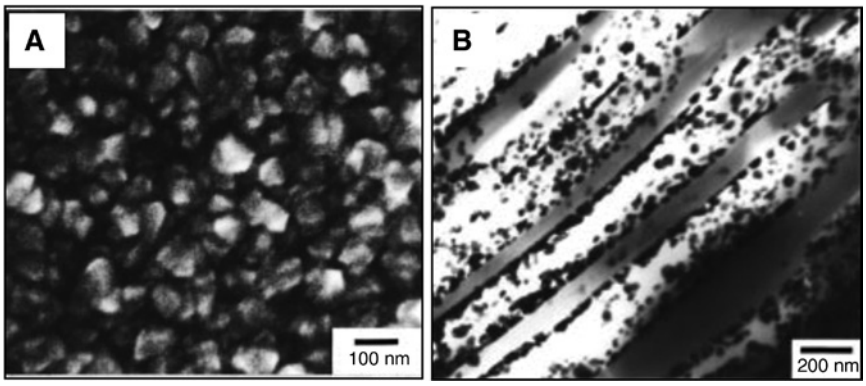

Figure 3: The first reported SFCD of metal Pt film onto silicon wafer (A) and porous alumina (B). Reprinted with permission from Watkins JJ, Blackburn JM, McCarthy ThJ, *Chem. Mater.* 1999, 11, 213–215 [33], Copyright 1999 American Chemical Society.

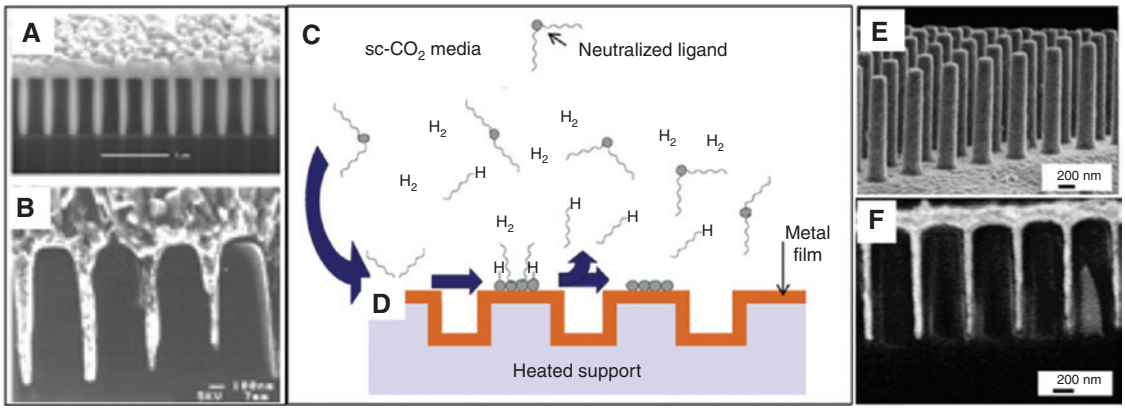

Figure 4: Conformal Cu film deposition onto etched Si support via the cold wall reactor method. (A, B) Complete filling with Cu of high-aspect-ratio features of <100 nm in width; (C, D) sketch of H_2-assisted metallization in sc-CO_2; (E) Au pillars and (F) Au films deposited onto etched silicon wafers. Reprinted with permission from Zong Y, Watkins JJ, *Chem. Mater.* 2005, 17, 560–565 [43], Copyright 2005 American Chemical Society; and from Cabañas A, Long DP, Watkins JJ, *Chem. Mater.* 2004, 16, 2028–2033 [44], Copyright 2004 American Chemical Society.

(Figure 3B). An effective metallization of a porous solid can be provided by separately controlling the transport (via a solution) and deposition mechanisms (via a chemical reducing agent).

Considering the nanotechnology challenges, design of nanostructures with control over the size of nano-objects, distribution, defect-free and a high-aspect-ratio feature fill, a new concept of deposition using a cold wall reactor was later developed [34].

2.1.1 Cold wall reactor

When the metal deposition occurs entirely on a heated substrate (T>200°C) in a reactor with walls having a much lower temperature (~60°C), through the reduction with H_2 of a sc-CO_2 soluble metal precursor, the approach is known as *cold wall reactor concept*, introduced for the first time by the Watkins group [34, 42, 43]. Through this method, device-quality copper and nickel films were deposited onto planar or etched silicon substrate heated at a temperature >250°C and yielding complete filling of high-aspect-ratio features <100 nm in width (Figure 4A, B). This concept also affords selective film growths, by using a seed layer (e.g. Pd as catalytic clusters) with a controlled spatial distribution of nucleation sites and a pure metal film, free from any organic ligands (C, F, or O) coming from the precursor decomposition. At a lower temperature (depending on the metal type, e.g. 200°C for Cu and 60°C for Ni), a seed layer on the support is necessary to act as a catalyst to start the nucleation of metal, while at higher temperatures (>225°C for Cu and >120°C for Ni) metal nucleation occurs without the need for catalysts. The reactivity of different metal precursors was tested [43, 44], showing that, in the absence of H_2, only Cu_2O film was forming, while the presence of H_2 as reducing agent leads to pure Cu film. It was demonstrated that H_2 also reacts with the organic ligand from precursors (dimethyl acetylacetonate {(acac)

$Au(CH_3)_2$}, cyclopentadienyl {$(Cp)_2Ni$}, cyclooctadiene-dimethyl {$(COD)Pt(CH_3)_2$} [44] or bis(2,2,6,6-tetramethyl, 3,5 heptadionato 1,5-cyclooctadiene-Ru(tmhd)$_2$cod) [45], neutralizing it and assisting their desorption from the substrate, in the presence of sc-CO_2, therefore avoiding the oxide formation and the film contamination with carbon and oxygen (Figure 4C). Studying the kinetics of metal deposition in sc-CO_2 [45], it was found that the film growth rate follows zero-order kinetics for both precursors (>0.06 wt.%) and hydrogen concentration (>0.26%) over various experimental conditions. Moreover, the rate-determining step appeared to be the surface reaction of protonation (Figure 4C) between both adsorbed hydrogen atoms and ligands (dissociated from surface adsorbed precursor) [43]. In addition, the by-products formed from these ligands, such as cyclooctadiene and cyclopentane, will have a negative first-order effect on growth rate, thus avoiding contamination with carbon and oxygen [45]. Unfortunately, this does not occur for CVD processes. Even when a dynamic vacuum method was used [46], promoting the release and elimination of the carbonyl part from the metal precursor, deposition assisted by vacuum ultraviolet irradiation of the precursor (2-methoxy-2,6,6-trimethylheptane-3,5-dionate) vapor [47] or low-pressure CVD of a single source precursor ([$nBu_2Ga(\mu$-$EtBu_2)2GanBu_2$], where E=P or As) [48], it was found that the deposited film has contamination with carbon, due to the decomposition of the precursor's ligand, and oxygen. Moreover, if the interest is to deposit films formed with small NPs (<50 nm), supercritical deposition is a better choice; by CVD, features >100 nm are obtained [46–48] and for higher material crystallinity additional steps are mandatory, but not in SFCD.

Similarly, using the concept of SFCD, metals such as Au [44] (Figure 4E, F), Ru [45], or metal oxide films, e.g. pure single-phase oxides of HfO_2, ZrO_2, and TiO_2 or mixed oxidation state materials in the cases of cerium, tantalum, niobium, and bismuth oxides [49, 50], were deposited.

Considering film deposition on a substrate as an inorganic-inorganic interface, we would like to draw the readers' attention to several issues that need to be considered. Film microstructure in terms of morphology, crystallinity, and thickness will be influenced by several factors related to both material and substrate [45, 50]:

1. The improvement of SFCD to yield conformal film deposition over a broad process window was the zero-order kinetics of the growth rate with respect to precursor concentration. In other words, high metal precursor concentration mitigates mass transport limitations and affords exceptional step coverage.
2. The type of material to deposit in direct contact with the substrate [50]. For instance, by using the cold wall reactor, the substrate's nature will induce variations in film thickness due to the change of thermal conductivity. If the film deposition is based on precursor hydrolysis, the presence of water molecules at the inorganic interface will be crucial. It was found that ceria films deposited using high H_2O/Ce molar ratios were smoother and denser than those deposited in the absence of water.
3. Films with grain sizes <10 nm even after annealing prepared by SFCD could show enhanced conductivity, especially when grain size becomes comparable to the dimension of grain boundaries resulting in the multiplication of interfaces and accumulation of defects that can lead to space charge effects [50].

Switching to hot wall reactor, metal or metal oxide NPs can be deposited or incorporated onto various types of substrates; the first reported Pt/polymer nanocomposite synthesis assisted by sc-CO_2 belongs to the Watkins group [51]. Two main concepts are used toward the formation of supported NPs, namely thermodynamically and kinetically controlled surface nanostructuration. On the basis of these concepts, reviews with very detailed information about the obtained NP-based structured materials were already published [3, 23–25, 35, 36]. Herein, attention will be focused on the chemistry at the inorganic or hybrid interfaces in these nanostructures, while gaining knowledge on its effect on the material's final physico-chemical properties. For a better understanding, a brief description of these concepts is proposed in the following subsections.

2.1.2 SCFD through thermodynamic control

Thermodynamic control of surface nanoengineering is based on the adsorption/sorption of metal precursor (already dissolved in SCF) onto the substrate followed by a wide variety of precursor transformations into its metal form: chemical reduction in a SCF with a reducing agent, chemical reduction with pure hydrogen at elevated pressure, thermal reduction in a SCF, thermal decomposition in an inert atmosphere, or chemical conversion with hydrogen or air at atmospheric pressure [3, 23–25, 35, 36, 45].

1. Thermal reduction at atmospheric pressure in an inert atmosphere: metal precursor(s) is (are) adsorbed onto a support, converted to their metal form, and the growth takes place by surface diffusion of the metal atoms and/or precursor molecules resulting in smaller spherical NPs.
2. Chemical reduction in sc-CO_2 with hydrogen: depending on the metal type, the particle nucleation and growth

during chemical reduction differ. The reduction of Pt or Pd precursors with H_2 in sc-CO_2 was determined to be autocatalytic, the NPs acting as nucleation sites, while H_2 reacts with the adsorbed precursor's molecules. Therefore, NPs continue to grow, coating the surface and forming dispersed NPs within a porous structure.

Note that other reduction methods have also been considered to be combinations of the previously mentioned ones, such as chemical reduction in pure H_2 or thermal reduction in sc-CO_2.

Metal, metal oxide, or binary metal NPs can be deposited onto various inorganic or organic substrates following the above-described procedure (Figure 5A). In the case of binary NP deposition [2], two paths could be followed: the simultaneous deposition (Figure 5C) of the metal precursors or a subsequent deposition (Figure 5A, B).

Various metal-organic precursors can be used, the most employed being β-diketone complexes. For the adsorption step, the precursor solubility data are of great importance, some of them being already available in the literature [52–55]. Whatever the nanostructured material – inorganic or hybrid – the investigation of both the kinetics and thermodynamics of precursors' adsorption or sorption processes is crucial. Their determination is based on the measurements of adsorption isotherms and concentration decay curves [56–58]. The adsorption or sorption kinetics are governed by the mass transfer either of the precursor in SCF or of the fluid on the surface or into the pores of the substrate. The thermodynamics of adsorption is generally quantified by an adsorption isotherm, i.e. the concentration of the precursor in the sc-CO_2 phase vs. its concentration in the solid phase. The isotherm is useful to control the organometallic uptake of the substrate, equivalent to metal loading. The slope of the adsorption isotherm is a measurement of the affinity between the precursor and the substrate. It was found that the obtained particles' size, distribution, and morphology depend on multiple factors, including the reduction method, nature of the substrate, type of the precursor and amount of precursor on the surface of the substrate, reaction temperature and time, etc. [23, 25, 35, 36]. In the following, we are presenting some selected examples of interesting inorganic and hybrid nanostructures prepared via SFCD's thermodynamic control.

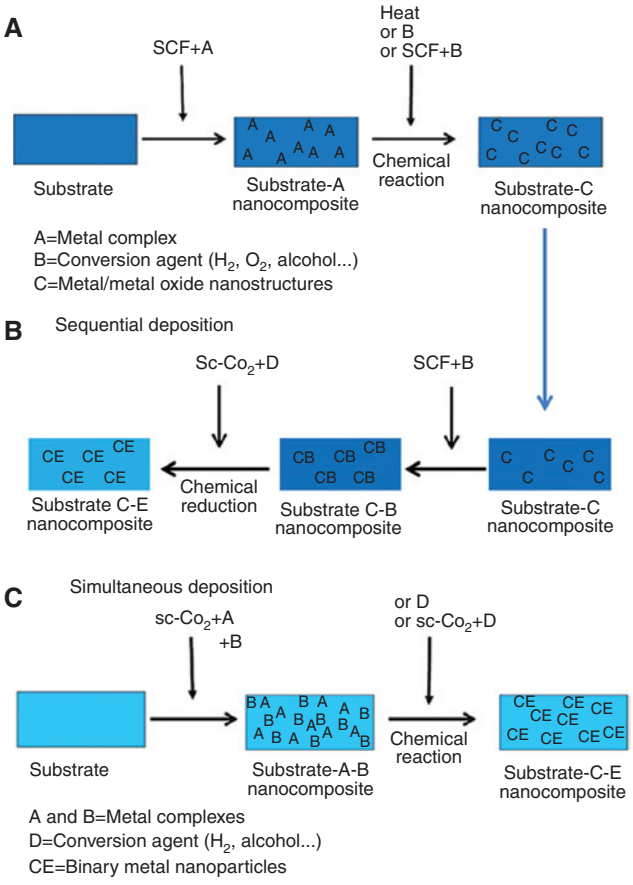

Figure 5: Thermodynamic control of SFCD for preparing NP-based structured materials: (A) metal or metal oxide NPs; (B, C) binary metal nanocomposites. Reprinted with permission from Bozbag SE, Erkey C, *J. Supercritical Fluids* 2015, 96, 298–312 [23], Copyright 2015 Elsevier.

2.1.2.1 Inorganic-inorganic interfaces

Intense research work was focused on metal (Pt, Pd, Cu, Ru, etc.) NP-based nanostructuring. Single metal or metal mixtures can be deposited onto various supports, e.g. on ceramic foams [59, 60], carbon black or aerogels, nanotubes, graphene [61–68], or oxide such as γ-alumina, silica/silica aerogels, Nafion 112 films [69], etc.; for each material, a specific precursor and an adapted procedure is used. Prior to deposition, an investigation of the phase behavior and the precursor solubility is usually made to determine the optimum temperature and pressure range for SFCD. Small Pt NPs (around 3 nm) with narrow size distribution were deposited onto ceramic foams coated with a layer of tin dioxide as supports (Figure 6A) (no interaction between Pt and the support) showing higher catalytic activity compared to conventional deposition of Pt by means of aqueous impregnation. By a simultaneous deposition, Pt and Cu were deposited onto ceria-coated ceramic foams [60]. It was found that the CeO_2 coating consisted of small NPs – <20 nm – showing an improved mobility of lattice oxygen and thus the appearance of oxygen vacancy known to stabilize late transition metal NPs by forming a strong metal-support bonding. The outcome is that the ceria layer was penetrated by the dissolved copper complexes, leading to close contact between copper and ceria [60], thus explaining the very

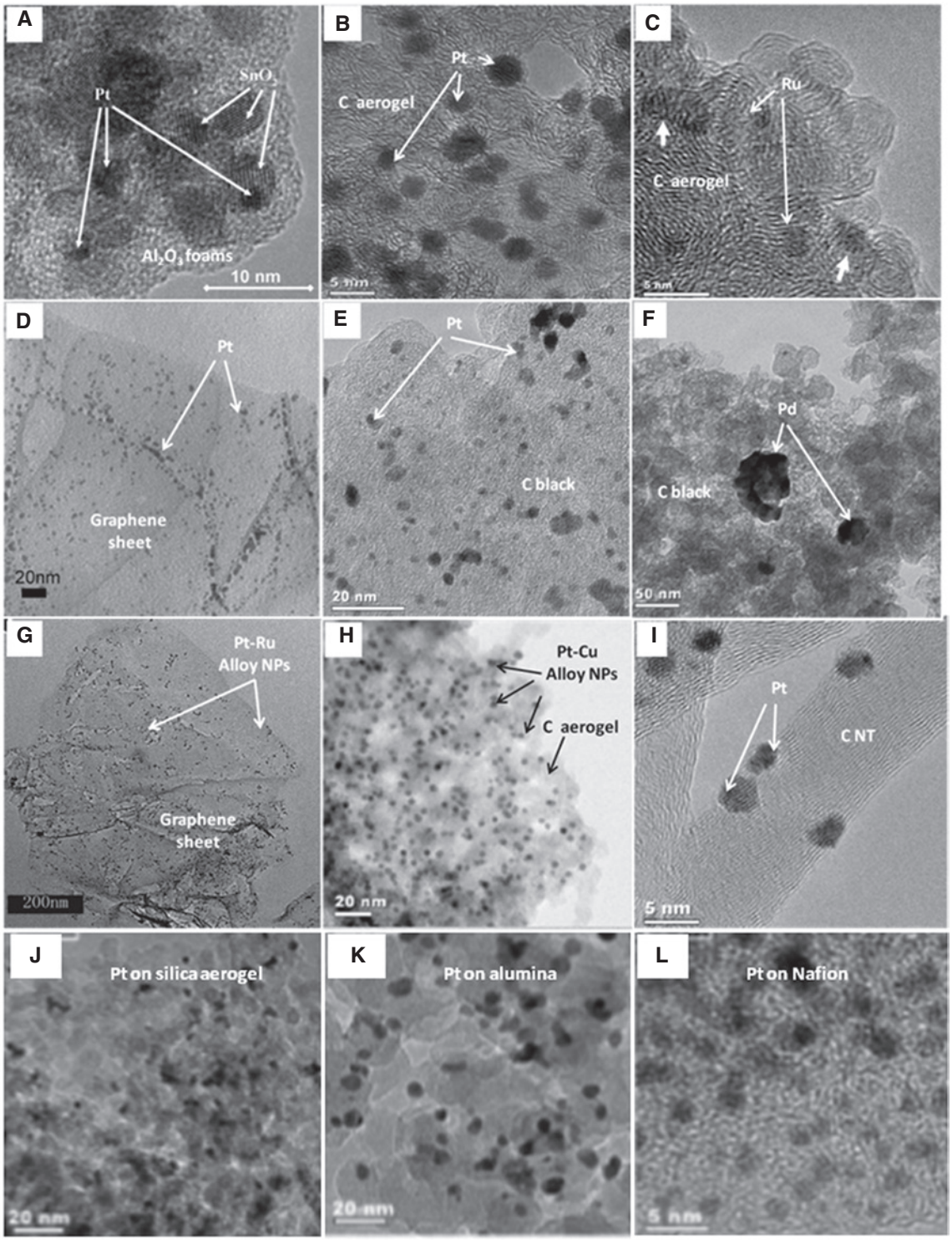

Figure 6: Different metal NPs deposited onto ceramic foams, carbon type, oxide type, or Nafion film supports with thermodynamically controlled SFCD [61–66, 69]. In all the presented cases, pure metal phases were prepared with no presence of interface compound. Reprinted with permission from Bozbag SE, Unal U, Kurykin MA, Ayala CJ, Aindow M, Erkey C, *J. Phys. Chem. C* 2013, 117, 6777–6787 [61], Copyright 2013 American Chemical Society; from Zhang Y, Kang D, Aindow M, Erkey C, *J. Phys. Chem. B* 2005, 109, 2617–2624 [62], Copyright 2005 American Chemical Society; from Cangül B, Zhang LC, Aindow M, Erkey C, *J. Supercrit. Fluids* 2009, 50, 82–90 [63], Copyright 2009 Elsevier; from Bayrakceken A, Cangul B, Zhan LC, Aindow M, Erkey C, *Int. J. Hydrogen Energy* 2010, 35, 11669–11680 [64], Copyright 2010 Elsevier; from Zhao J, Yu H, Liu Z, Ji M, Zhang L, Sun G, *J. Phys. Chem. C* 2014, 118, 1182–1190 [65], Copyright 2014 American Chemical Society; from Zhao J, Zhang L, Xue H, Wang Z, Hu H, *RSC Adv.* 2012, 2, 9651–9659 [66], Copyright 2012 Royal Society of Chemistry; and from Zhang Y, Kang D, Saquing C, Aindow M, Erkey C, *Ind. Eng. Chem. Res.* 2005, 44, 4161–4164 [69], Copyright 2005 American Chemical Society.

good catalytic activity. On the other hand, Pt precursor was fully reduced to metal Pt, and it was supposed that it acts as either a catalyst to reduce the $Cu(tmhd)_2$ or as a dopant for the CuO/CeO_2 catalyst. Other works were reported for Pt NPs (Figure 6B, D, E, I, J–L) deposited onto C-type substrates (e.g. carbon aerogels, carbon black, nanotubes, or graphene) [61–66] or oxide and Nafion [69]. With these examples, it can be noticed that even considering the same metal, different reduction methods and different substrates will critically influence the average size, distribution, and morphology of the Pt NPs onto/within the carbon, oxide framework, or Nafion film. Different Pt sizes were obtained when different reduction methods were employed [70]. The simultaneous deposition of Pt and Cu precursors onto C aerogels yielded an alloy of Pt-Cu (Figure 6H) and depending on the two metal ratios, the size was varying accordingly – larger when the Cu content was higher [61]. Depositing Ru NPs onto carbon aerogels (Figure 6C), very small (~4 nm) homogeneously distributed NPs were prepared, the mean size being dependent on the reduction temperature [62]. When Pt was combined with Pd, similar observations were reported for metals deposited onto carbon black [63, 64]. Pd alone (Figure 6F) yielded very irregular NP distribution onto support with a very broad size distribution (3–100 nm), whereas Pt NPs (Figure 6E) were homogeneously distributed with a size ranging from 2 to 6 nm. Adding Pt to Pd increases the homogeneity and decreases the NP size. Depositing Pt on graphene (Figure 6D), small (~2 nm) monodispersed NPs are obtained, with the loading percentage being controlled by varying the precursor/graphene ratio [65]. Thus, a maximum loading of 80 wt.% was achieved, uniformly distributed without any significant changes in the Pt NPs size, and the material showing enhanced catalytic activity compared to Pt deposited on carbon nanotubes (CNTs) or carbon black. Combining two precursors (salt type) of Pt and Ru, very small (~3 nm) Pt-Ru alloy NPs (Figure 6G) were uniformly distributed on graphene, with Ru atoms partially dissolved in the Pt fcc lattice [66]. Depositing Pt on the surface of CNTs (Figure 6I) [67], the NPs adopted a roughly hemispherical morphology of 2 nm. By studying the adsorption isotherms, it was found that the precursor's affinity is higher for CNTs than for sc-CO_2, allowing controlling precisely the metal loading onto the support.

Nanostructured materials with controlled morphology were obtained by depositing Pd (Figure 7A, C) [56]

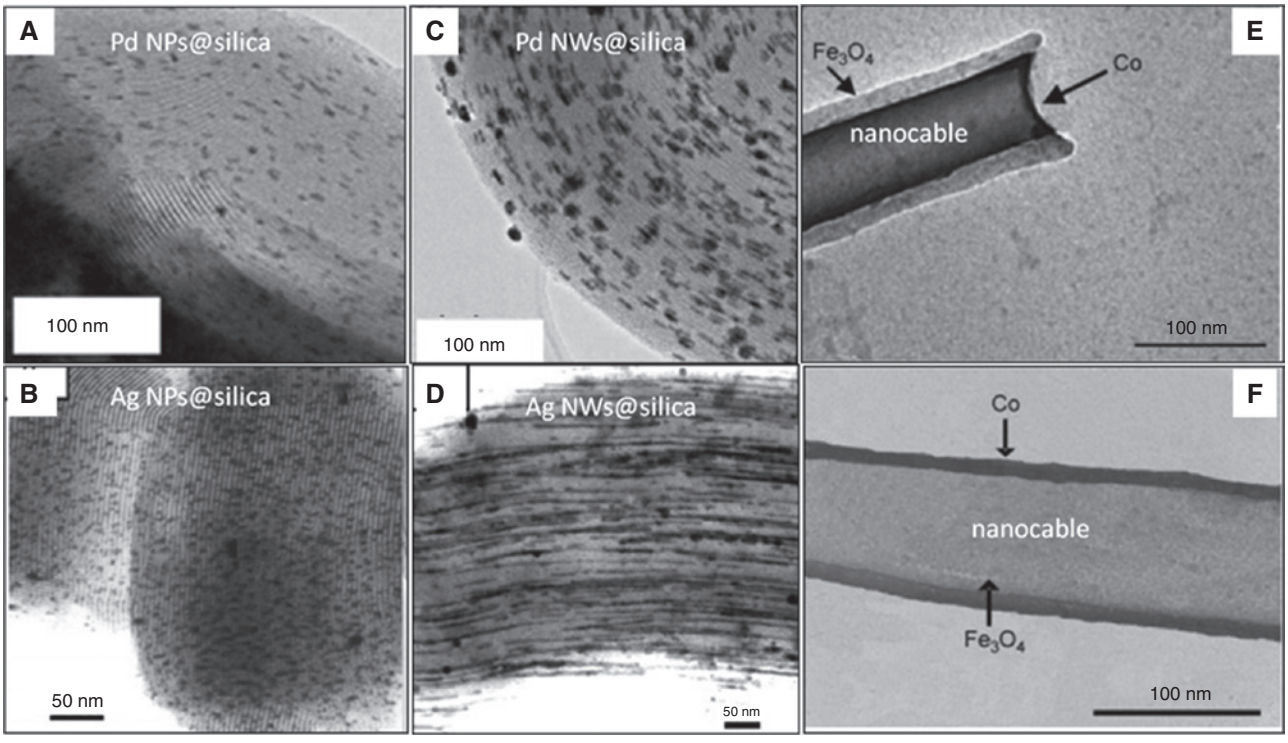

Figure 7: Mesoporous silica filled with NPs of Pd (A) and Ag (B) at lower precursor concentration; increasing the metal loading, nanowires of Pd (C) and Ag (D) are formed within the pores. Reprinted with permission from Aschenbrenner O, Kemper S, Dahmen N, Schaber K, Dinjus E, *J. Supercrit. Fluids* 2007, 41, 179–186 [53], Copyright 2007 Elsevier; and from Zhao J, Yu H, Liu Z, Ji M, Zhang L, Sun G, *J. Phys. Chem. C* 2014, 118, 1182–1190 [65], Copyright 2014 American Chemical Society, respectively. (E, F) For Co@Fe_3O_4 or Fe_3O_4@Co nanocables. Reprinted with permission from Daly B, Arnold DC, Kulkani JS, Kazakova O, Shaw MT, Nikitenko S, Erts D, Morris MA, Holmes JD, *Small* 2006, 2, 1299–1307 [71], Copyright 2006 J. Wiley.

and Ag (Figure 7B, D) [68] metals within mesoporous silica. It was observed that at low metal loading, small NPs were formed (Figure 7A, B), while an increase of the metal loading or impregnation time led to nanowires (NWs) formation (Figure 7C, D). NPs were confined within the pore of the support and therefore their growth was limited in two dimensions, turning into small NWs. More unusual nanostructuration, for instance core-shell type nanocables (Figure 7E, F), where the core is an oxide and the shell is a metal or *vice versa*, can also be prepared [71].

2.1.2.2 Inorganic-organic interface

Türk et al. studied the influence of organic ligand being part of the metal precursor over the metal NPs' deposition onto porous alumina support [72]. Cyclooctadiene-stabilized Pt complexes containing different perfluoroalkane chains, [Pt(cod)Me-(C_nF_{2n+1})], namely *n/i*-C_3F_7, *n*-C_4F_9, *n*-C_6F_{13}, *n*-C_8F_{17}, where *n*=normal and *I*=branched chains, were considered. The type of organic ligand, its size, and configuration could change the solubility of the Pt complexes in sc-CO_2, thus influencing the Pt NP size, size distribution, and metal loading. Surprisingly, the Pt NP size (<3 nm) and size distribution were not influenced by the substitution of the CH_3 end group by the C_nF_{2n+1} end groups; however, their effect was observed on the Pt loading, the highest (67 wt.%) being for [Pt(cod)Me_2] – the reference. By varying the precursor's concentration, the formation of NPs agrees with classical nucleation theory, i.e. smaller NPs for lower precursor concentration. Pt(COD)Me_2 dissolved in sc-CO_2 and impregnated on β-cyclodextrin followed by reduction with H_2 [73] yielded Pt NPs of different sizes (labeled as <20, <100, and >100 nm). Their shapes depend on the experimental conditions, such as the precursor and support mixing conditions and the precursor reduction strategy (Figure 8A–C).

Using the same approach, gold NPs were incorporated into various polymers (Figure 8D–F) [74], and it was found

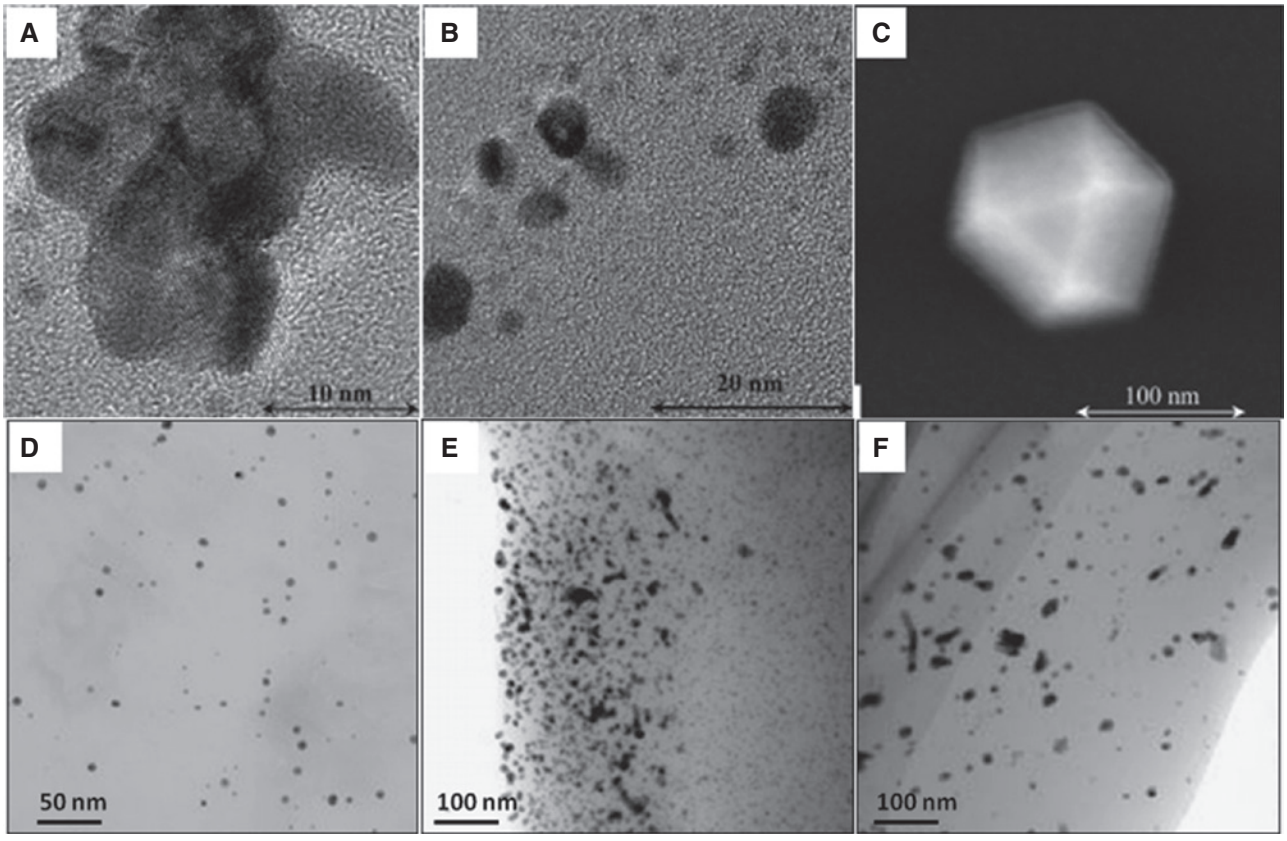

Figure 8: Nanocomposites where the metal NPs morphology is influenced by different experimental conditions: Pt NPs incorporated in β-cyclodextrine with diameters of (A) <20 nm, (B) <100, and (C) >100 nm depending on the procedure. Reprinted with permission from Pelka J, Gehrke H, Esselen M, Türk M, Crone M, Bräse S, Müller T, Blank H, Send W, Zibat V, Brenner P, Schneider R, Gerthsen D, Marko D, *Chem. Res. Toxicol.* 2009, 22, 649–659 [73], Copyright 2009 American Chemical Society. Au NPs incorporated in different types of polymers as (D) PTFE, (E) polyamide, and (F) polypropylene. Reprinted with permission from Wong B, Yoda S, Howdle SM, *J. Supercrit. Fluids* 2007, 42, 282–287 [74], Copyright 2007 American Chemical Society.

that the NP morphology (size, shape, and dispersion) was critically influenced by the type of polymer:

1. Small homogeneously dispersed Au NPs were obtained when the polymer was poly(tetrafluoroethylene) (PTFE) (Figure 8D).
2. Considering polyamide, a gradient of size and NP dispersion was observed, the larger NPs (~19 nm) being close to the surface whilst the smaller ones (~3 nm) dispersed in the center (Figure 8E).
3. In polypropylene, large erratic non-circular particles of 20 nm were prepared (Figure 8F).

An explanation for this could be attributed on the one hand to a different interaction between the polymers and precursors/NPs and, on the other hand, by the diffusion of different sc-CO_2/precursors within the polymer. It was assumed that polyamide and polypropylene might have a lower affinity than PTFE to sc-CO_2 and hence the precursor uptake, the nucleation, and particle growth being significantly affected, as experimentally observed.

To summarize, the use of the SFCD route via thermodynamic control allows achieving nanoengineering of complicated architectures. Starting with metal oxide/metal films deposited on solid substrates – engineered or not – continuing with supported NPs of many types and finishing with embedded NPs in various materials, a satisfactory control over nano-objects morphology can be obtained. Even so, this approach generally requires long and multistep procedures. An alternative approach is the kinetically controlled SFCD.

2.1.3 Kinetically controlled SCFD

2.1.3.1 Inorganic-inorganic interfaces

The thermodynamically controlled approach focuses on (i) selecting the right precursor to favor adsorption onto the substrate and (ii) wait for enough time to promote this adsorption. Oppositely, the kinetically controlled approach pays no particular attention to these considerations. The latter concept was developed by our group and was first reported for Cu NPs deposited on silica spheres in supercritical CO_2/alcohol mixture [32]. Another important aspect to be mentioned is that there are no requirements for precursor adsorption onto the substrate, such as the case of copper NP deposition onto silica beads, where the considered hydrophobic copper hexafluoroacetylacetonate precursor cannot be adsorbed onto hydrophilic silica surface. Additionally, the contacting time is generally in the order of 1 h, which is much shorter than the adsorption time in the thermodynamically approach. Thus, kinetically controlled SCFD is based on the homogeneous nucleation and heterogeneous growth (coalescence of nuclei or direct reduction of precursor over the existing) induced by a chemical reaction [32, 37] (Figure 9), being validated by numerical simulation [75]. Reduction of a metal precursor, generally bearing β-ketonate counteranions, takes place usually in the presence of H_2 with or without alcohols, and additionally, a surfactant could be used [18]. It was found that in the absence of any interaction between the NPs and support, the experimental parameters such as temperature (T), residence time (t_s), and mass ratio of Cu(hfac)$_2$·H_2O/silica spheres (r_m) influence the deposited NP size in the range 5–17 nm, and also the coverage of the silica surface (40–80%, Figure 10A). We would like to underline that, whatever the percentage of Cu NP surface coverage is, the NPs are monodispersed on the support surface, without any NP agglomeration.

Employing similar conditions with another metal, for instance Pd, different deposition behaviors were found [18]. Small metal Pd NPs were formed but they were deposited in large agglomerates of spherical shape (Figure 10B–E). This behavior could be explained by the Pd's autocatalytic behavior, creating active nucleation. By adding an amine-type surfactant as a weaker reducing agent, the Pd NP size is not changing considerably as it should be expected in a more reducing media; however, it affects the morphology and dispersion on the silica surface, creating more homogeneous nucleation sites. Changing the silica support with more active ones, such as CeO_2, TiO_2, and Fe_2O_3, a similar Pd NP size (around 9 nm) was obtained, preserving at the same time the agglomeration trend [18].

When Pd NPs were deposited onto magnesium-scandium alloy ($Mg_{0.65}Sc_{0.35}$), 10-nm Pd NPs were formed and the same deposition trend was observed [76]. The platelet-like morphology of this support hampers an easy observation of the Pd/ $Mg_{0.65}Sc_{0.35}$ interface, while an earlier work of our group reported the absence of an interphase with palladium on Mg support (Figure 11A–D), but with the presence of an interphase with copper (i.e. $MgCu_2$) and nickel (i.e. Mg_2Ni) [19] (Figure 11E–H). It was found that all three metals, Pd, Cu and Ni, were deposited onto the Mg surface either as aggregates or single NPs, in agreement with other previous observations, concordant with the bimodal kinetic surface nanostructuration model. It is worth noticing that, contrary to the surface modification of spherical particle supports (200–500 nm) with monodispersed metal NPs, the supports showing lower specific surface area (Mg crystals, Mg-Sc platelets, or silica-irregular shapes) and so less available surface for the deposition will promote the coalescence mechanism of the deposited supported NPs.

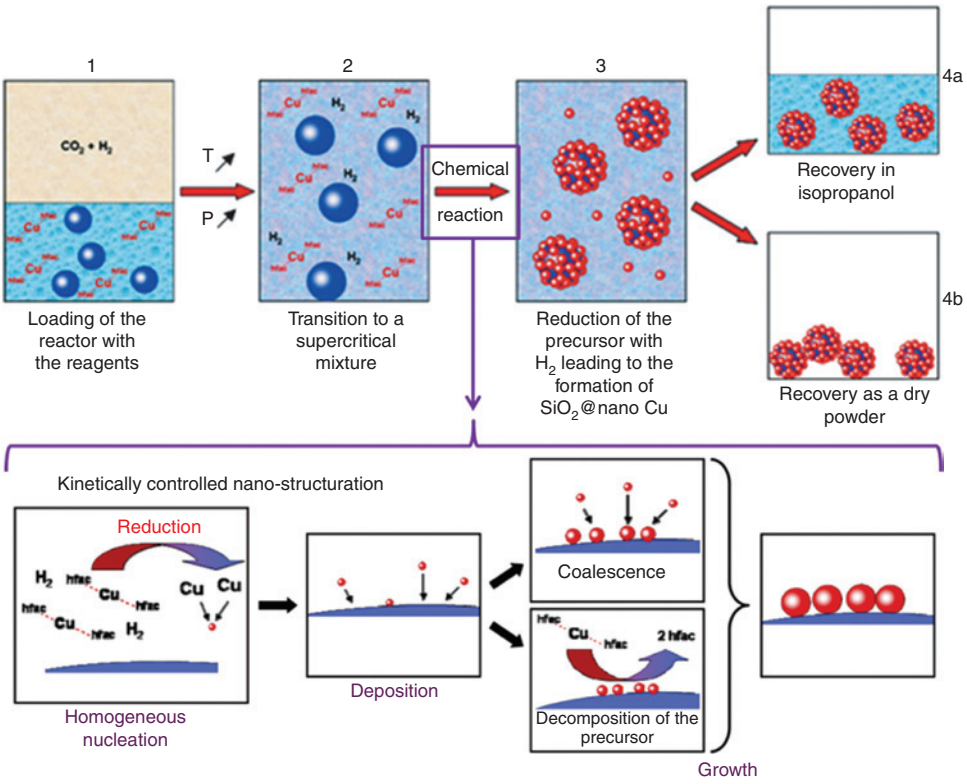

Figure 9: Sketch of the kinetically SFCD controlled surface nanostructuration process. Reprinted with permission from Marre S, Cansell F, Aymonier C, *Nanotechnology* 2006, 17, 4594–4599 [32], Copyright 2006 IOP Science.

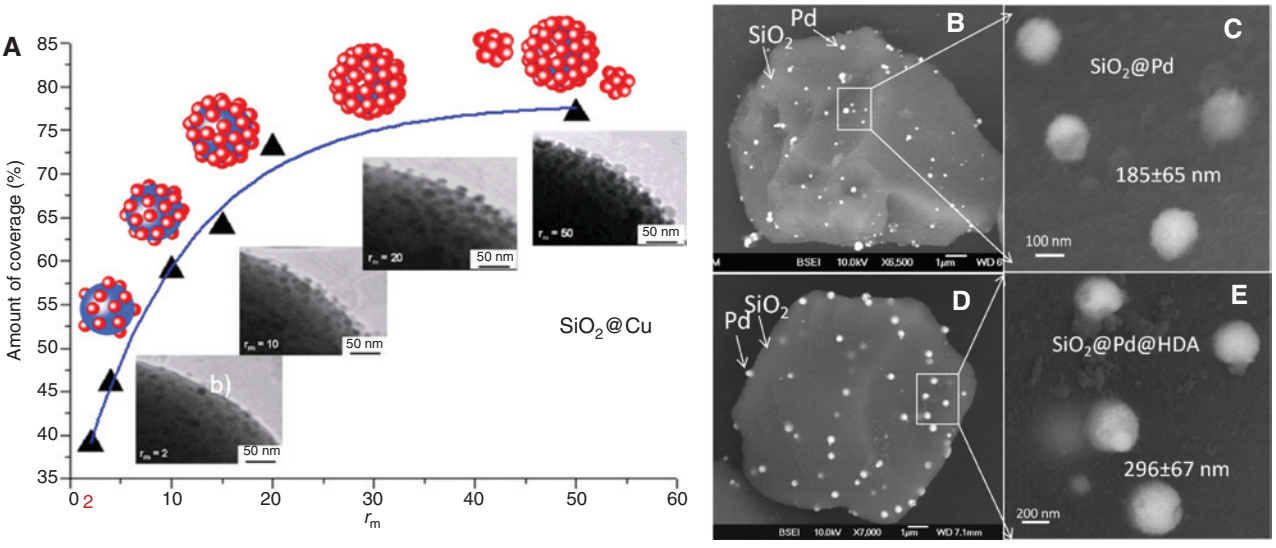

Figure 10: Examples of inorganic (A–C) or hybrid (D, E) nanostructures. (A) Silica surface decorated with monodispersed Cu NPs, with the surface coverage increasing when the mass ratio (r_m) between Cu precursor and silica is increasing. Reprinted with permission from Marre S, Cansell F, Aymonier C, *Nanotechnology* 2006, 17, 4594–4599 [32], Copyright 2006 IOP Science. (B, C) Silica surface decorated with large spherical agglomerates (~200 nm) made of small (~8 nm) Pd NPs. (D, E) Silica surface decorated with larger more uniform spherical agglomerates (~300 nm) made of small (~8 nm) Pd NPs in the presence of an amine-type surfactant. Reprinted with permission from Pascu O, Cacciuttolo B, Marre S, Pucheault M, Aymonier C, *J. Supercrit. Fluids* 2015 [18], Copyright 2015 Elsevier.

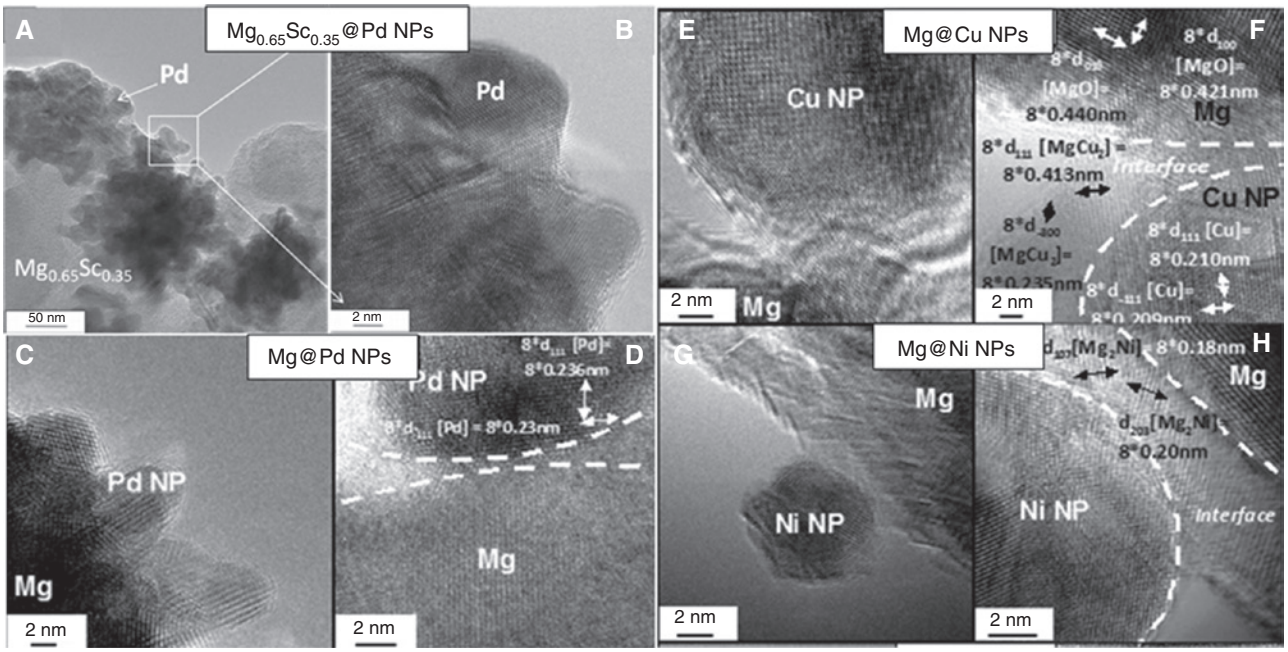

Figure 11: Examples of inorganic nanostructures with the absence (A–D) or presence (E–H) of an interphase compound. (A, B) Magnesium-scandium alloy decorated with agglomerated Pd NPs. Reprinted with permission from Couillaud S, Kirikova M, Zaïdi W, Bonnet JP, Marre S, Aymonier C, Zhang J, Cuevas F, Latroche M, Aymard L, Bobet JL, *J. Alloys Compd.* 2013, 574, 6–12 [76], Copyright 2013 Elsevier. (C, D) Magnesium surface decorated with agglomerated Pd NPs. Reprinted with permission from Aymonier C, Denis A, Roig Y, Iturbe M, Sellier E, Marre S, Cansell F, Bobet JL, *J. Supercrit. Fluids* 2010, 53, 102–107 [19], Copyright 2010 Elsevier. (E, F) Magnesium surface decorated with aggregates/single Cu NPs with the formation of an interphase compound of $MgCu_2$ [19]. (G, H) Magnesium surface decorated with aggregates/single Ni NPs with the formation of an interphase compound of Mg_2Ni [19].

More interestingly, thanks to the SFCD approach, an interphase between metal NPs and their support can be formed, opening interesting perspectives for the preparation of nanostructured materials with enhanced properties. Specifically, in the case of hydrogen storage, we have demonstrated that this interface is at the origin of a significant cyclability improvement of the materials [77].

2.1.3.2 Inorganic-organic interfaces

A recent work reported the deposition of Pd NPs [from $Pd(hfac)_2$ precursor] onto cellulose NCs (CNXLs) in sc-CO_2 in the absence of H_2, only using the cellulose support as reducing agent (due to OH surface groups) [78]. It was found by X-ray photoelectron spectroscopy (XPS) measurements that Pd^{2+} appears at the interface between metal Pd and CNXLs, and a rather strong bond keeps the Pd NPs attached to the surface of CNXLs. However, when the NPs exceed the critical diameter of around 13 nm, NPs start detaching from the surface, possibly because the cellulose cannot longer sustain the NPs mechanically above this size.

Using other supercritical solvents than sc-CO_2 (e.g. EtOH, hexane) [78–80], interesting materials can be prepared by controlling the morphology (size, shape) of the NPs with the reaction temperature, pressure, time, precursor concentration, and presence of surfactants. Employing either an organic surfactant, as reducing and/or stabilizer, or seeds of another material, anisotropic NPs such as nanorods and NWs can be prepared. Using oleylamine (OAm) as both a reducing and a capping agent for controlling the crystallite size and phase, spherical or rod-like $LiMnPO_4$ NPs were synthesized in batch mode in ethanol at supercritical conditions (T=250–400°C, p=38 MPa, 4–10 min) [79]. Although ethanol is a reducing agent, in the absence of OAm, both phases of $LiMnPO_4$ and Li_3PO_4 (as impurity) were formed, while in the presence of OAm pure $LiMnPO_4$ was obtained. This result suggested that OAm – as a surfactant – provides a suitable reducing atmosphere for controlling the oxidation of Mn^{2+} to Mn^{3+}. Moreover, it has been found that OAm was acting also as a capping agent, decreasing the $LiMnPO_4$ NP size down to 7 nm and at the same time directing an anisotropic growth (Figure 12A) via a typical surfactant-assisted oriented attachment growth mechanism (Figure 12B, C).

NWs are an interesting class of nanostructured materials, with 1D quantum confinement and able to connect components in a nanointegrated system. An interesting approach to prepare NWs using SCFs is

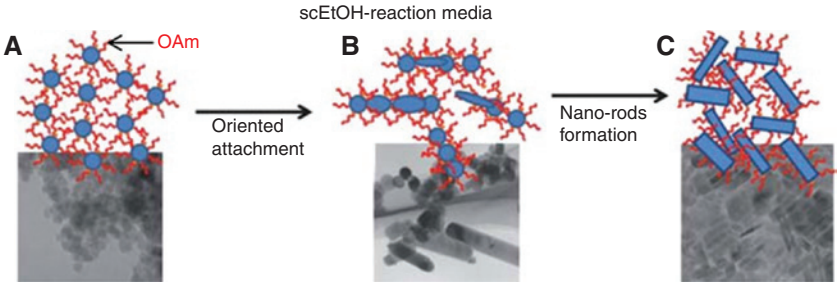

Figure 12: Surfactant-assisted oriented attachment growth mechanism for $LiMnPO_4$ NPs obtained from supercritical ethanol/oleylamine system in batch mode. Reprinted with permission from Rangappa D, Sone K, Zhou Y, Kud T, Honma I, *J. Mater. Chem.* 2011, 21, 15813–15818 [79], Copyright 2011 Royal Society of Chemistry.

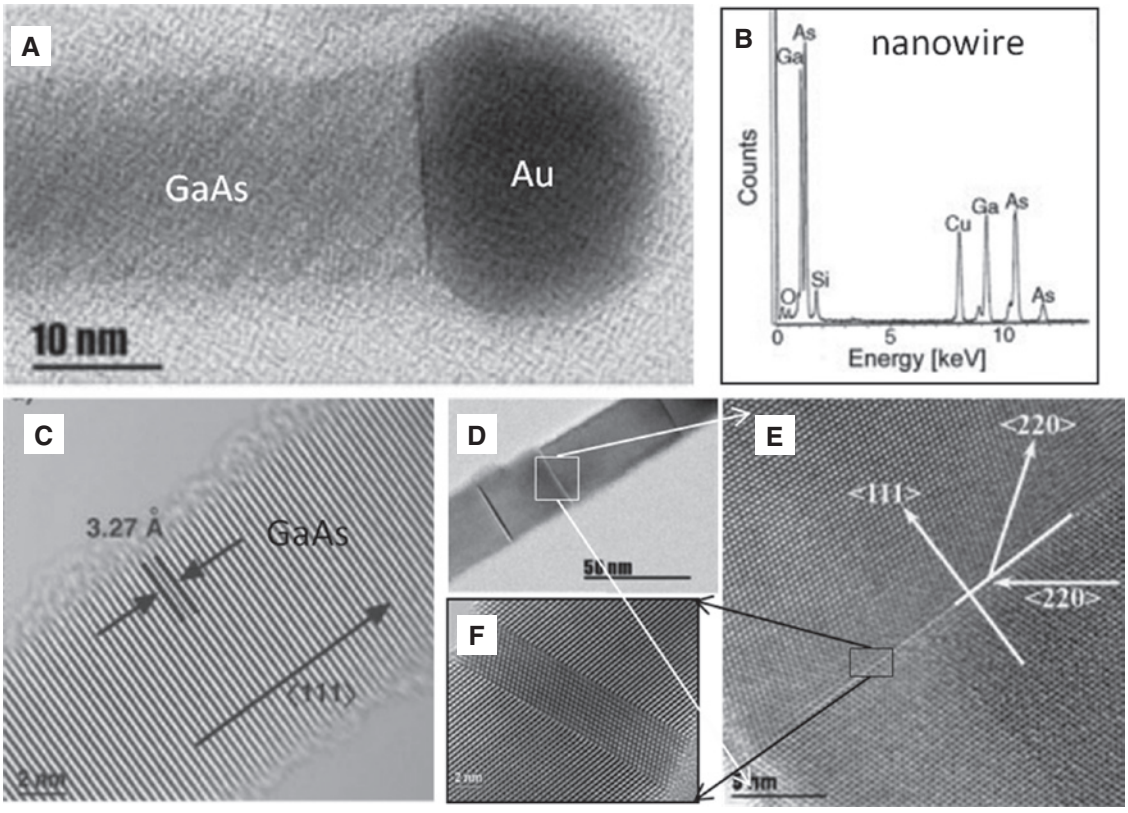

Figure 13: Seed-oriented NW growth via the SCF-liquid-solid route. (A) Thiol-capped Au seed nanocrystal for growing GaAs NWs; (B) XPS data of NWs, showing the presence of Si (from precursor) as doping atom in NW; (C) single crystal GaAs NW with diameter <15 nm; (D) multitwinned GaAs NW with diameter >15 nm; (E, F) high resolution of twinning faults. Reprinted with permission from Davidson III FM, Schrinker AD, Wiacek RJ, Korgel BA, *Adv. Mater.* 2004, 16, 646–649 [80], Copyright 2004 J. Wiley.

the SCF-liquid-solid NW growth [80, 81]. GaAs NWs (Figure 13) were prepared in sc-hexane (T=500°C, p=37 MPa) in the presence of 7-nm dodecanthiol-stabilized Au NC seeds [80]. An important issue to be taken into consideration with this kind of approach is the precursor degradation kinetics. Indeed, the precursor type chosen has to provide the need for NW formation limiting the particles' growth (Figure 13A). An important point is that NWs with a diameter >15 nm presents twinning faults, the defects being confined to a single plane (111) (Figure 13D, E), while no defects were observed in smaller-diameter NWs (Figure 13C). Between the Au seed and the GaAS NWs, no interface compound is observed (Figure 13A) but XPS analysis (Figure 13B) showed the presence of Si [from the precursor, $As(SiMe_3)_3$] as a doping non-metal element in the NWs during the supercritical process. Similar doping/

incorporation with a non-metal atom coming from the precursor/reaction media was observed by our group, on Pd NPs with C or H incorporated during synthesis in supercritical acetone [20].

An analogous SCF-liquid-solid process was used to prepare high yields of single-crystalline Si and core-shell Ge/SiO_x NWs directly nucleated from the stainless-steel or titanium reactor wall and grown in metal reactor cells under high-pressure SCF conditions (sc-CO_2) [81]. This wall nucleation was confirmed by the presence of Fe and Ti at the base of the NWs, with NWs growth proceeding through extrusion from the base region. Furthermore, the NW formation occurred only by mixing diphenylsilane/germane precursors with a coordinating solvent, trioctylphosphine (TOP), suggesting that the addition of hydrocarbon ligands to sc-CO_2 is acting both as capping ligand for the already formed NCs and steric stabilizer to the emerging nuclei during the reaction [81].

Other types of hybrid nanostructured materials prepared via kinetically controlled SFCD are metal NPs stabilized within organic matrices such as polymers [82] or ionic liquids [83–85]. The preparation method relies on the reduction of a metal precursor in a CO_2 solution containing an insoluble polymer. Reduction of the metal with H_2 leads to small NCs, with good polydispersity, stabilized by the polymer. This hybrid material is recovered as a dry powder, ready to use and free of any organic solvents with the possibility of being resuspended in an appropriate solvent. It is worth mentioning that through this approach, there is no need to have the chemicals (hyperbranched polymer and metal precursor) soluble in sc-CO_2. The following formation mechanism was proposed (Figure 14A): (i) sc-CO_2 diffuses into the powder (step 1) and swells the polymer, which becomes liquid at the bottom of the reactor (step 2). (ii) The metal precursor is dissolved by the liquid polymer and due to the presence of H_2, coming together with CO_2 molecules, the subsequent reduction to metal takes place (step 2) followed by the NPs formation and stabilization by the hyperbranched polymers (step 3). During depressurization, the ligands (from the precursor) together with the CO_2 molecules are released from the powder, yielding

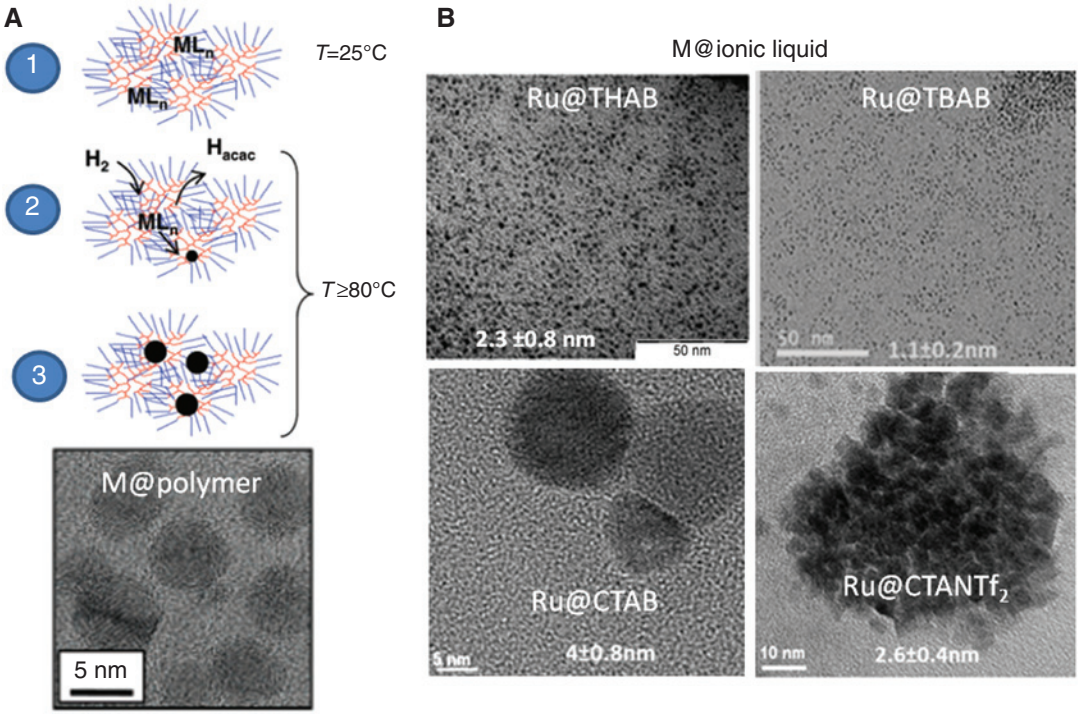

Figure 14: Hybrid nanostructuration via the preparation of metal NCs stabilized by organic molecules insoluble in sc-CO_2. (A) Proposed formation mechanism of Pd@polymer dry powders. Reprinted with permission from Moisan S, Martinez V, Weisbecker P, Cansell F, Mecking S, Aymonier C, *J. Am. Chem. Soc.* 2007, 129, 10602–10606 [82], Copyright 2007 American Chemical Society. (B) Metal NCs stabilized by different quaternary ammonium salts, such as THAB (tetrahexylammonium bromide) (reprinted with permission from Cimpeanu V, Kocevar M, Parvulescu VI, Leitner W, *Angew. Chem. Int. Ed.* 2009, 48, 1085–1088 [83], Copyright 2009 J. Wiley), TBAB (tetrabutylammonium bromide), CTAB (cetyltrimethylammonium bromide), and $CTANTf_2$ (cetyltrimethylammonium bis(trifluoromethylsulfonyl)imide) (reprinted with permission from Liautard V, Pascu O, Aymonier C, Pucheault M, *Catal. Today* [85], 2015 Copyright 2015 Elsevier).

dry nanostructured materials (NPs stabilized by hyperbranched polymers), ready to be used. By changing the polymer to onium salts (powder at room temperature), the same principle of hybrid nanostructuration can be considered, due to the significant melting point depression of onium salts in the presence of compressed CO_2, thus forming ionic liquids. This was demonstrated by the preparation of NCs of noble metals (Pd, Pt, Ir, Rh, and Ru) stabilized by quaternary ammonium salts (with different melting temperatures and structures), which were used as efficient nanocatalysts [83–85]. It was found that the metal NCs' physico-chemical properties, such as size, size distribution, organization, and surface chemistry, could be controlled by varying the type/structure of stabilizer (Figure 14B), metal type, or experimental conditions.

Kinetically controlled SFCD leads to high-quality materials with useful properties. A larger and more sophisticated garden of nanostructures can be achieved with the continuous SCF route, presented in the next section of this review paper.

2.2 CSFS

As we have presented thus far, nanostructuration based on SFCD, when an inorganic or organic support is used, takes place in batch mode. Although the batch approach affords highly crystalline nano-objects, its main limitation is the required long residence time (from minutes to hours), and in the case of monodispersed NPs the impossibility to control nucleation, growth, and subsequent functionalization steps, separately. An optimization for designing highly versatile multifunctional nanostructures are the continuous SCF approaches, taking benefit from thermodynamic fluid properties, hydrodynamics, and chemical reaction kinetics with or without surfactant or template in short times (from seconds to minutes). A sketch of the continuous process is presented in Figure 15. The basic concept consists in flowing the reactive fluid in a coiled tubular reactor fed with high-pressure pumps and pressurized with a back-pressure regulator valve [26, 27], the nanostructures being recovered either as dry powders (using an online filter) or in solution.

In the tubular reactor, the possible chemical reactions that could occur are hydrothermal reactions in supercritical conditions (hydrolysis and dehydration of metal salts and metal-organic precursors), thermal decomposition of metal-organic precursors, reduction/oxidation of metal salts or metal-organic precursors with H_2, or sol-gel (with hydrolysis and condensation) [26, 27]. The control of the chemical reactions within the reactor is directly linked to the synthesized materials' characteristics (morphology, structure, composition, and organization/stability), which can be achieved by choosing specific operating parameters: solvent nature (water, alcohol, ammonia, mixtures, etc.), pressure, temperature, reagent nature and concentration, reactor technology (single tubing or co-flow), residence time in the reactor, and additive agents (co-solvent, catalyst, surfactants, etc.). These parameters are controlled as follows: (i) pressure – using an appropriated

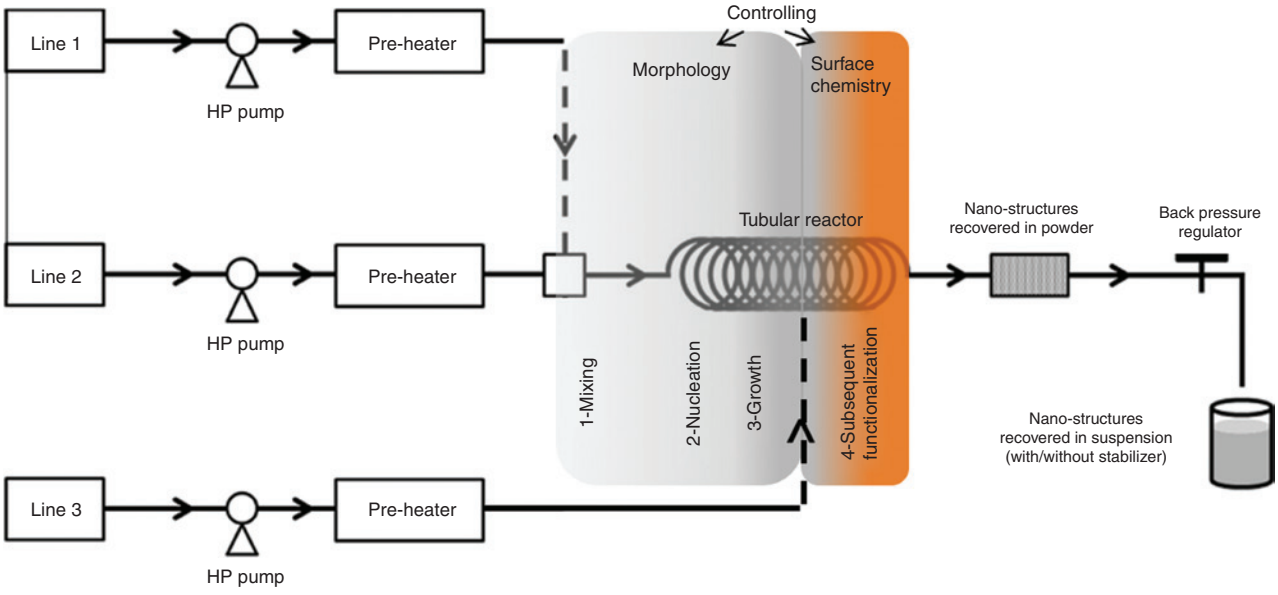

Figure 15: General sketch of CSFS with control over nucleation, growth, and subsequent functionalization steps. Reprinted with permission from Philippot G, Elissalde C, Maglione M, Aymonier C, *Adv. Powder Technol.* 2014, 25, 1415–1429 [26], Copyright 2014 Elsevier.

back-pressure regulator and pump(s); (ii) temperature in the reactor – using preheaters and a reactor heating system; (iii) residence time in the reactor – by controlling the flow rates (Q_m), the reactor volume (tubing type), temperature, and pressure (related with the fluid density); and (iv) concentrations of reagents of the feed solutions [27].

Control of the surface chemistry of nano-objects can be achieved by a proper choice of solvent nature, precursor type, and stabilizer agent. It was found, and later discussed, that if the reaction media is an alcohol, it can also act as a stabilizing agent, modifying the NPs surface chemistry by its attachment onto the surface. Additionally, the presence of an organic ligand could affect the NPs morphology (size, shape, composition, and size distribution), organization, and stability. The organic stabilizer could be *in situ* or *ex situ* introduced, the former functionalization being done by two different ways: (i) the stabilizer is introduced from the beginning in the reactor, mixed with the precursor solution (Figure 15, 1 – mixing step) and (ii) the stabilizer solution could be introduced downstream into the reactor, just after the nucleation/growth steps (Figure 15, 4 – subsequent functionalization). When considering *ex situ* functionalization, the stabilizer is added to the vessel where nano-objects are recovered as suspensions, based on the fact that highly reactive nano-objects are obtained at the end of the continuous reactor. In the CSFS approach, the predominant type of materials prepared is hybrid nanostructures, but also inorganic ones are the subjects of intense researches. The next paragraphs will be devoted to exemplify the two types of materials prepared using three concepts, specifically naked nanostructures in the absence of any additives, *in*(*ex*) *situ* functionalization with an organic stabilizer, and *co-flow* with multifunctionality.

2.2.1 Naked nanostructures

2.2.1.1 Inorganic-inorganic interface

Using the continuous approach, one-pot synthesis of high-quality nano-objects (well crystallized, narrow size distributed, pure, stoichiometric, etc.) can be achieved in a very short time (from few seconds to few minutes) and with a good reproducibility. Supercritical water is an attractive reaction environment for hydrothermal crystallization of metal oxide particles due to the radical changes of its properties (e.g. density, dielectric constant, etc.) around the critical point, therefore influencing the phase behavior of supercritical water-light gas (O_2, H_2, etc.) mixtures, the reaction equilibrium/rate, leading to the synthesis of new materials or specific particle morphologies. The Adschiri group was pioneer in the continuous supercritical hydrothermal synthesis, preparing a myriad of materials. Briefly, the method developed by Adschiri et al. [86] consists in feeding the reactor with one stream of aqueous metal salt solution (at room temperature), which is allowed to mix with a hot preheated water stream (at a temperature above the reaction temperature), allowing fast heating of the reactive fluids to the desired temperature conditions. This leads to a rapid reaction in the reactor and afterward, the outlet solution is rapidly quenched, particles being collected in the effluent after passing through a filter (to remove the largest particles). Hydrothermal reactions proceed faster at supercritical conditions than in subcritical water because the lower dielectric constant results in an enhancement of the reaction rate and thus smaller particles can be obtained. Similarly, particle morphology can be controlled with temperature and pressure, especially around the critical point, due to the variations of the dielectric constant and the ionic product of water, exemplified with the boehmite (AlOOH) case. It was found that AlOOH particle morphology was determined by selective adsorption of positively charged species, $Al(OH)^{2+}$ or $Al(OH)_2^+$, on the negatively charged surface of the AlOOH crystals at chemical equilibrium. By small changes in temperature and pressure, this equilibrium was modified, thus affecting the chemical species distribution and therefore the crystal habits [86]. It is important to recall that the formation of a homogeneous phase for supercritical solution and light gases (e.g. O_2 or H_2) provides a uniform oxidizing or reducing environment promoting the oxidizing/reducing capability of the reaction environment, leading to the control of the material composition. Through this procedure, complex metal oxide particles were prepared, such as barium hexaferrite ($BaFe_{12}O_{19}$), metal-doped oxide [$Al_5(Y+Tb)_3O_{12}$, YAG/Tb], and lithium cobalt oxide ($LiCoO_2$). Barium titanate ($BaTiO_3$) is yet another example of material worthy to be presented. Intense research has been devoted to prepare this material by various methods [26], and the SCF approach can be considered. Starting from barium hydroxide and titanium dioxide as precursors, fine NPs were prepared by supercritical hydrothermal synthesis (400°C and 30 MPa) [87]. A pH >13 was necessary to obtain a pure $BaTiO_3$ phase, as this condition is required to dissolve titanium dioxide in water, releasing the titanium ions readily to react with barium ions. Through rapid heating, small particles in the range 10–50 nm or larger (up to 150 nm) were obtained (Figure 16A). By changing the supercritical media (water+ethanol), the precursor type (barium and titanium isopropoxides – dissolved in ethanol), and the type of chemical reaction, namely supercritical sol-gel, in the temperature range 150–380°C at 16 MPa pressure, ultra-fine barium titanate ($BaTiO_3$) and also barium strontium titanate

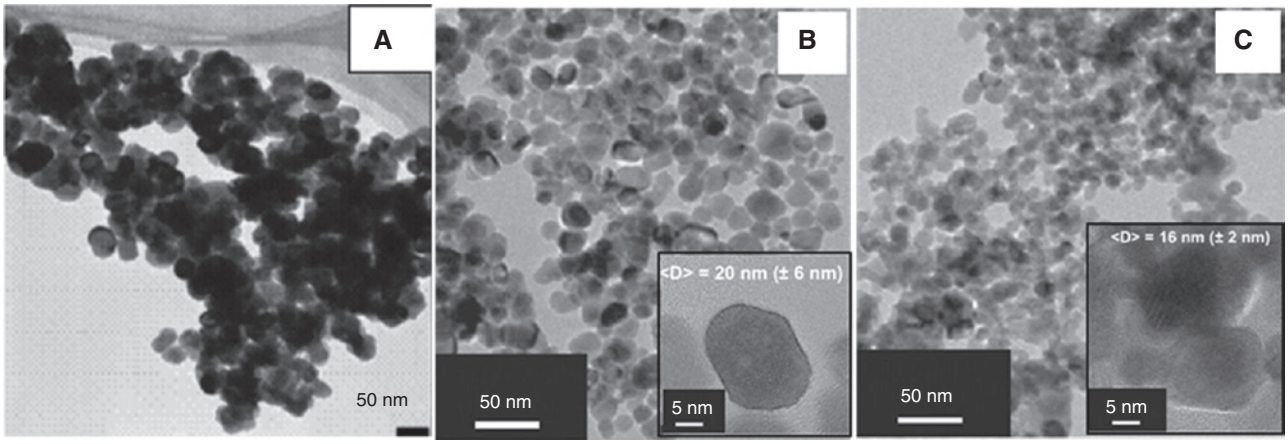

Figure 16: $BaTiO_3$ and $Ba_{1-x}Sr_xTiO_3$, $0 \leq x \leq 1$, particles synthesized by two different supercritical chemical routes: (A) hydrothermal reaction ($BaTiO_3$) (reprinted with permission from Atashfaraza M, Shariatvy-Niassar M, Ohara S, Minami K, Umetsua M, Naka T, Adschri T, *Fluid Phase Equilibr.* 2007, 257, 233–237 [87], Copyright 2007 Elsevier) and (B) sol-gel route in supercritical mixture (water+EtOH) for $BaTiO_3$. (C) $Ba_{0.6}Sr_{0.4}TiO_3$ NCs obtained through sol-gel routes in H_2O/EtOH mixtures. Reprinted with permission from Philippot G, Jensen KMO, Christensen M, Elissalde C, Maglione M, Iversen BB, Aymonier C, *J. Supercrit. Fluids* 2014, 87, 111–117 [88], Copyright 2007 Elsevier.

($Ba_{1-x}Sr_xTiO_3$) [88] powders with a crystallinity as high as 90% have been successfully prepared without barium carbonate contamination [26, 89]. The particles exhibited sizes of ~40 nm with -OH defects, similar to the NPs synthesized by hydrothermal reaction. By optimizing the process [85] (higher temperature, 1 min residence time), the NP size was decreased to 20±6 nm (for $BaTiO_3$, Figure 16B) and even further by increasing the amount of strontium ($Ba_{1-x}Sr_xTiO_3$, $0 \leq x \leq 1$), e.g. 16±2 nm for $Ba_{0.6}Sr_{0.4}TiO_3$ (Figure 16C). To understand the NP formation mechanism, *in situ* synchrotron powder diffraction was coupled with *ex situ* analyses such as Fourier transform infrared spectroscopy (FTIR), Raman spectroscopy, XPS, X-ray diffraction, and high-resolution transmission electron microscopy (HR-TEM) [86]. A reduction of -OH surface defects when strontium was added was revealed, this being attributed to the presence of less dissolved ions in solution, because of the Sr-O stronger ionic bond, which was impeding the ions' dissolution. Owing to the sol-gel mechanism, the surface -OH is responsible for the reaction, but -OH loss will decrease the ability of the precursor to react at the surface, thus limiting the particle growth. Inorganic systems – as core-shell-type particles – were prepared by precipitating Ni shell over Fe_3O_4 nuclei in subcritical water by hydrogen reduction from $Ni(CH_3COO)_2$ aqueous solution [90]. Magnetite nuclei were first formed by the hydrothermal synthesis from $FeSO_4$ aqueous solution through a Fe^{2+}+"phen" complex (phen=1,10-phenanthroline), the latter compound inhibiting the hydrolysis of Ni^{2+} at higher temperatures, therefore avoiding NiO formation. The thickness of the Ni shell over the Fe_3O_4 nuclei can be increased by increasing the reaction temperature and the Ni/Fe molar ratio in the feed solution. Unfortunately, no further details about the inorganic interface could be found in the report. Another type of solvent to produce inorganic nanostructured materials is supercritical ammonia [91]. By performing thermal decomposition of metal precursors in a supercritical ammonia-methanol mixture in a temperature range 170–290°C at p~16 MPa, nitrides (Cr_2N, Co_2N, Fe_4N, Cu_3N, and Ni_3N), metal (Cu), and oxides (Al_2O_3, TiO_2, and Ga_2O_3) can be prepared. With the exception of pure Cu_3N cubic monocrystal particles of 10 µm, the other nitride particles obtained were organized in shapeless aggregates of a few micrometers constituted of crystalline nanodomains. Their composition varied depending on the metal type from pure nitrides for Ni and Co to mixed oxy-nitrides for Fe and Cr. The preparation of nitrides at relatively low temperatures occurs for the metals when the Gibbs free energy of oxide formation is not too low (e.g. Cr, Co, Cu, Ni, and Fe) whilst oxides are obtained at very low free Gibbs energy (e.g. Ga, Al and Ti).

Depending on the final application, naked nano-objects could be of interest; however, it is difficult to have full control over their morphology, stability, and organization. As an alternative, *in situ*/*ex situ* functionalization can bring additional opportunities when specific properties are required.

2.2.2 *In situ*/*ex situ* functionalized nanostructures

2.2.2.1 *In situ*/*ex situ* functionalization via the hydrothermal route

The development of different morphologies and organization of oxides or bimetallic-based hybrid nanostructured

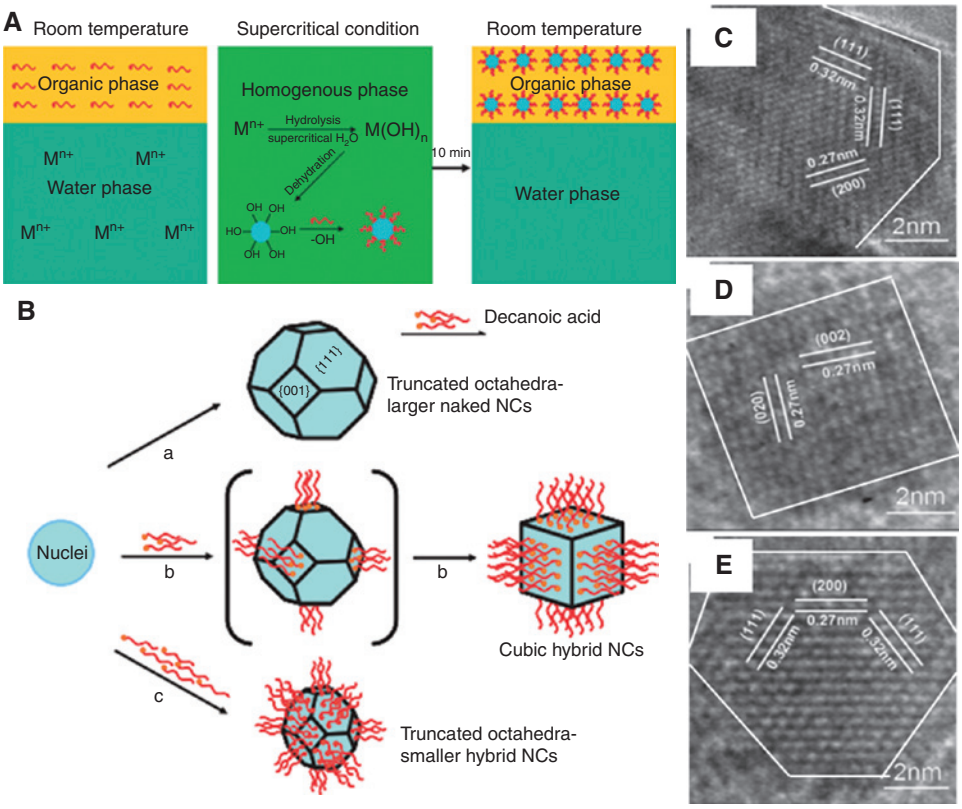

Figure 17: Batch supercritical hydrothermal synthesis of oxide-based hybrid nanostructures: (A) nanocrystals synthesis strategy; (B) growth mechanism influenced by organic surfactant; (C) CeO_2 NCs in the absence of surfactant; (D) cubic CeO_2 NCs when the surfactant concentration is low; and (E) hybrid CeO_2 NCs with a high surfactant concentration. Reprinted with permission from Zhang J, Ohara S, Umetsu M, Naka T, Hatakeyama Y, Adschiri T, *Adv. Mater.* 2007, 19, 203–206 [94], Copyright 2007 J. Wiley.

materials was achieved by the Adschiri [92–102] and the Türk [103–105] groups via a supercritical hydrothermal approach in the presence of organic stabilizers or clickable anchors. The Adschiri group method is based on the concepts of organic-solution phase and liquid-solid-solution phase synthetic transfer routes, where the organic surfactant plays a key role in the shape-controlled growth and organization/stability of oxide NCs. The NCs formation strategy is illustrated in Figure 17 and is based on the following:

1. Single crystals of <10 nm are formed during the supercritical hydrothermal process (Figure 17A).
2. The organic ligand molecules become miscible with the supercritical water, thanks to the low dielectric constant of water.
3. The NCs' growth is controlled by proper selection of the organic ligand molecules with selectivity to a specific inorganic crystal surface (Figure 17B).

The use of water, instead of organic solvents, provides a green chemistry route to prepare nanoblocks for advanced materials and devices [94]. In the case of ceria NCs, smaller surfactant concentration (decanoic acid) leads to cubic structures (Figure 18D), while increasing its concentration will form truncated octahedral NCs similar to the naked ones (Figure 17C) but smaller (Figure 17E) [94, 95].

Changing the surfactant type from a monoacidic to a diacidic one (hexanedioic acid), ceria NCs auto-assembled in cubic organizations were obtained due to an octa-coordination of the primary octahedral NCs with di-acidic surfactants forming a bridge at the hybrid interface (Figure 18) [96]. The two carboxyl groups of hexanedioic acid are bounded to the Ce atoms on the surface of octahedral CeO_2 NCs, preventing the growth of the primary octahedral NCs. HfO_2 NPs were prepared in similar conditions [98].

Using a surfactant with double functionalities, hydroxyl (-OH) and carboxylic (-COOH) groups, such as 3,4-dihydroxycinnamic acid (DHCA), different oxide morphologies, exemplified with Fe_3O_4 [99, 100] and HfO_2 [98], are achieved. Fe_3O_4 in the form of raspberry-like aggregates (Figure 19B, C), made of small magnetic NPs (~20 nm), were prepared under hydrothermal conditions

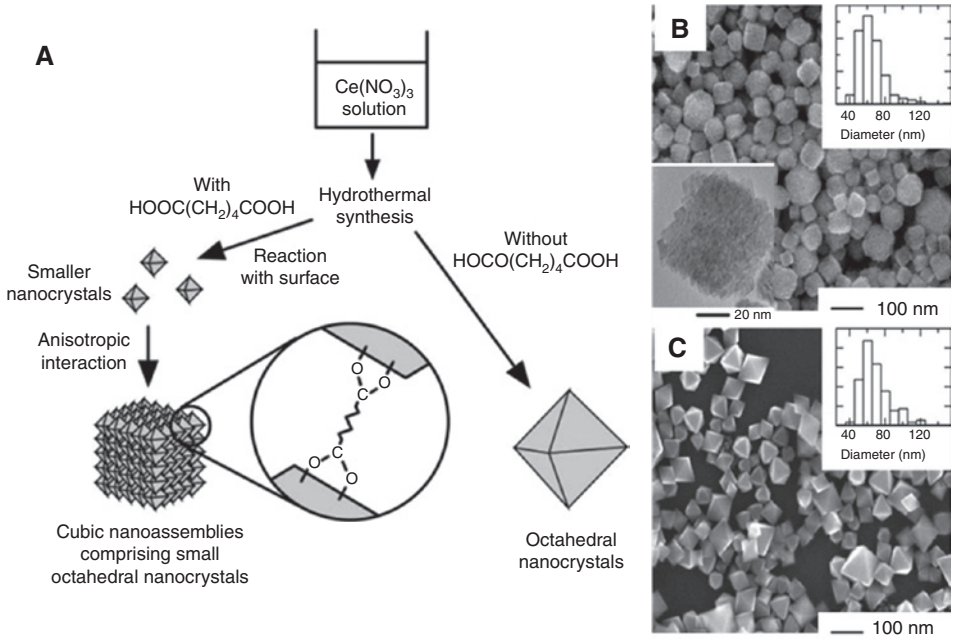

Figure 18: Principle of the hydrothermal synthesis of ceria NCs (A), in the presence (B) or absence (C) of hexanedioic acid. Reprinted with permission from Takami S, Ohara S, Adschiri T, Wakayama Y, Chikyow T, *Dalton Trans.* 2008, 5442–5446 [96], Copyright 2008 Royal Society of Chemistry.

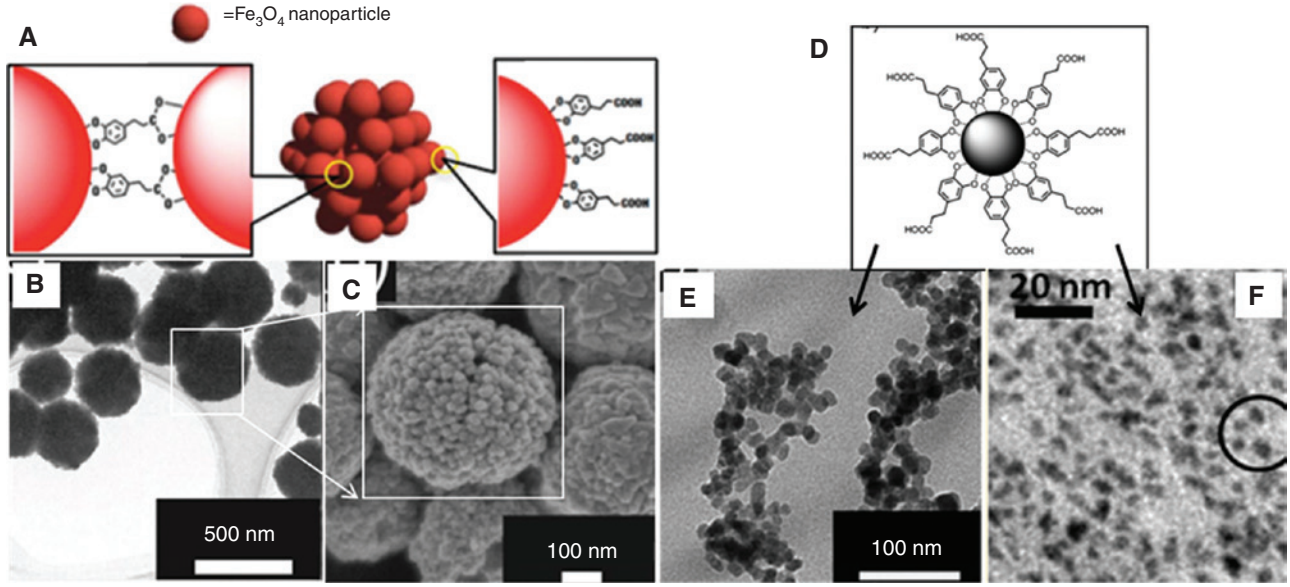

Figure 19: Hydrothermal synthesis of Fe_3O_4 (reprinted with permission from Togashi T, Naka T, Asahina S, Sato K, Takami S, Adschiri T, *Dalton Trans.* 2011, 40, 1073–1078 [99], Copyright 2011 Royal Society of Chemistry) and HfO_2 (reprinted with permission from Sahraneshin A, Asahina S, Togashi T, Singh V, Takami S, Hojo D, Arita T, Minami K, Adschiri T, *Cryst. Growth Des.* 2012, 12, 5219–5226 [98], Copyright 2012 American Chemical Society) NPs *in situ* functionalized with 3,4-dihydroxycinnamic acid surfactant. (A) Sketch of the formation mechanism of iron oxide aggregates, (B) TEM image of the aggregates, and (C) HR-SEM image of the raspberry-like aggregates made by small Fe_3O_4 NPs [99]. (D, E) Changing the synthesis parameters (T=350°C), monodispersed Fe_3O_4 NPs were prepared (~18 nm). (F) At similar conditions, 4-nm HfO_2 NCs were obtained [98].

at 200°C in the presence of DHCA. The NPs within the aggregates were connected by DHCA molecules to form the clusters (Figure 19A–C) and can be easily dispersed in water media, thanks to COOH groups on their surfaces. The clusters size ranging from 50 to 400 nm could be tuned by controlling the residence time without changing

the primary particle size [99] while keeping their superparamagnetic properties. Increasing the reaction temperature (in the range of 230–350°C), smaller monodispersed iron oxide NPs (10–18 nm) were obtained (Figure 19D, E) [100]. At similar hydrothermal conditions (T=350°C, p=16 MPa), HfO_2 NPs were prepared. It was found that the precursor solution alkalinity and the amount of DHCA – used as a multifunctional capping agent – were key factors for controlling the size and shape of the NCs, namely flower-like nanostructures (20 nm in diameter), polycrystalline nanoagglomerates (25 nm in diameter), and water-dispersible single NPs (4 nm in diameter) (Figure 19F) [98]. The double-functionality surfactants could act as strong bridges (covalently bonded) connecting the surface of two NPs and organizing them in aggregates with various morphologies.

Zinc oxide (ZnO) is yet another example of material synthesized by the hydrothermal route with or without organic stabilizer [101, 102] (Figure 20). Starting from nitrate precursor at supercritical water conditions, ZnO nanorods were prepared in the absence of organic surfactant [101] (Figure 20A). In most cases, the surfaces of the metal oxide NPs formed in hydrothermal conditions are covered by hydroxyl or ether groups, rendering them hydrophilic and thus dispersible in water. The surface hydrophilicity can be changed to hydrophobicity using reagents that can react with surface hydroxyl groups, such as alcohols, aldehydes, carboxylic acids, and amines [101, 102], and at the same time controlling the NP morphology (size, shape, and distribution), as exemplified in Figure 20B, C.

Research related to the synthesis and *in situ* continuous functionalization of iron oxide NPs in supercritical or near-critical water with groups that can undergo "click" reactions was reported in the last 3 years by the Türk group [103–105]. It is well known that iron oxide NPs' structure and properties strongly depend on their size, their history of formation, and the surrounding medium. On the basis of these considerations, the Türk group has investigated, using a conventional T union setup, the role of mixing ratio, fluid velocity (Figure 21A–C), and type of the precursor (Figure 21D–F) on the size distribution of both primary and agglomerated particles, colloidal stability [103]. Additionally, they performed a Raman spectroscopy study of the system directly in the aqueous dispersion, based on the fact that the properties of the iron oxides can be changed during the preparation steps [103]. It was found that the synthesis from pure aqueous iron(III) nitrate solutions exhibits a bimodal distribution of particles, but increasing the total mass flow rate and mixing ratio between precursor (metal salts) stream and supercritical water stream, the fraction of the larger population was decreased. By changing the iron(III) nitrate precursor with acidified mixtures of iron(II) acetate and iron(III) nitrate, much narrower particle/agglomerate size distributions were obtained. Moreover, the presence of a mixture of α-Fe_2O_3 and γ-Fe_2O_3 and/or ferrihydrite was detected using Raman analysis, showing that the structure and size of the synthesized particles can change upon drying, resulting in inaccurate results.

Further works [104, 105] were based on the *in situ* synthesis of iron oxide NPs with different types of carboxylic acids, such as hexynoic, hexanoic, and undecynoic acids, in order to undergo a second functionalization via "click chemistry". Knowing that the precursor and organic capping type influence the NPs morphology, surface reactivity – important for the *in situ* functionalization – was tested (Fe nitrate and citrate salts and also different mixing setups). It was found that a mixture of maghemite/magnetite and hematite NPs was obtained:

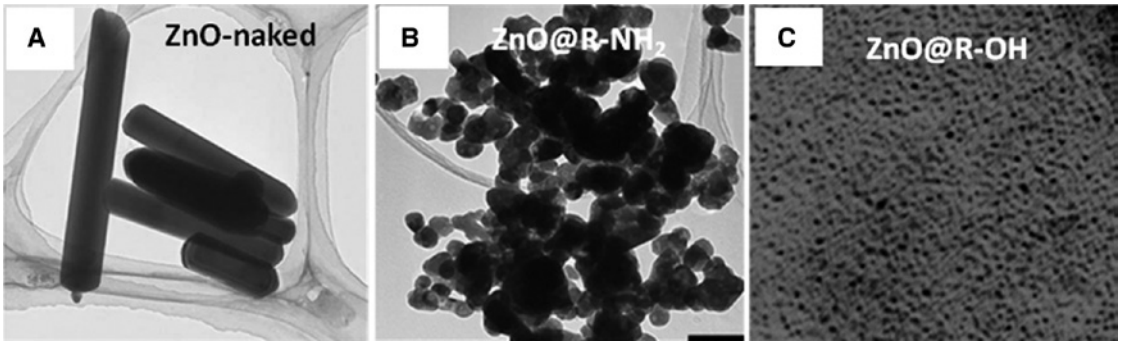

Figure 20: Hydrothermal synthesis of ZnO without (A) (reprinted with permission from Ohara S, Mousavand T, Sasaki T, Umetsu M, Naka T, Adschiri T, *J. Mater. Sci.* 2008, 43, 2393–2396 [101], Copyright 2008 Springer) or with different types of organic stabilizers, such as amine (B) or alcohol (C) (reprinted with permission from Mousavand T, Ohara S, Naka T, Umetsu M, Takami S, Adschiri T, *J. Mater. Res.* 2010, 25, 219–223 [102], Copyright 2010 Cambridge University Press).

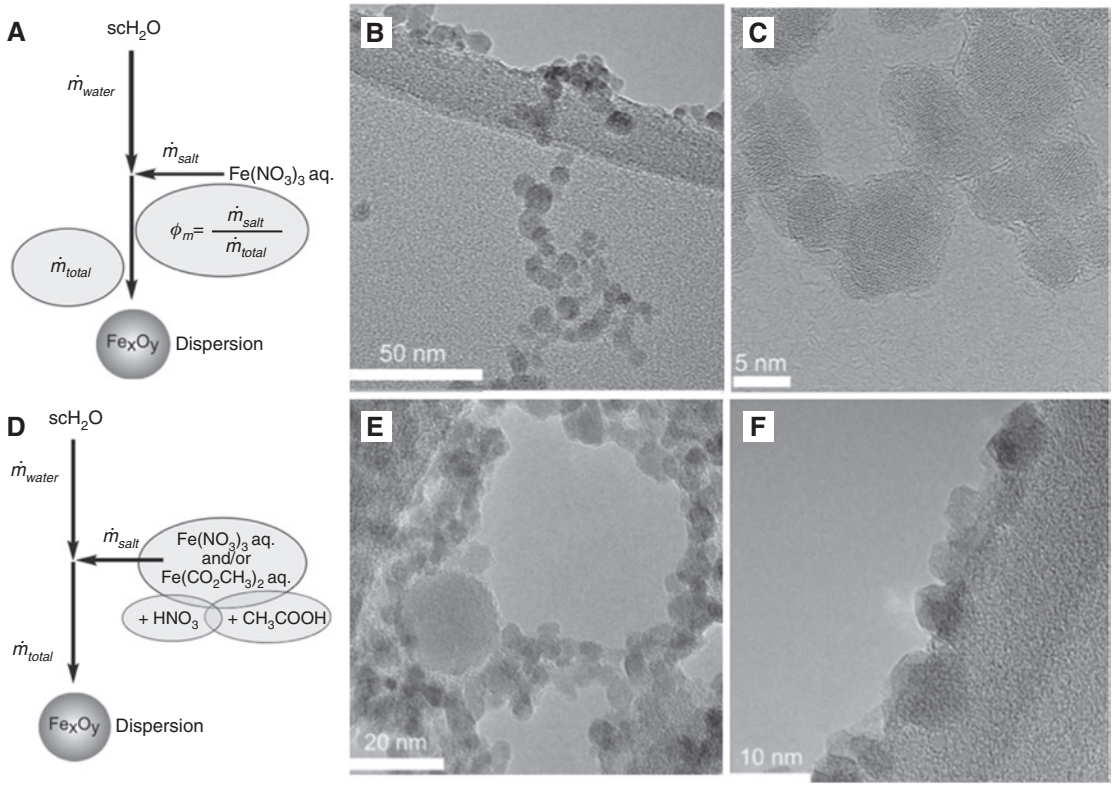

Figure 21: Iron oxide synthesized at different conditions (reprinted with permission from Daschner de Tercero M, Röder C, Fehrenbacher U, Teipel U, Türk M, *J. Nanopart. Res.* 2014, 16, 2350-1–2350-27 [103], Copyright 2014 Springer): mixing ratio, fluid velocity (A) at 3 kg/h (B) and 9 kg/h (C): different chemical compositions (D): mixture at 3 kg/h (E) and 6 kg/h (F).

larger (>50 nm) rectangular NPs of maghemite with smaller (~6 nm) spherical NPs of magnetite. The presence of surface acids thus allows a further coupling, opening new application opportunities.

2.2.2.2 *In situ*/*ex situ* functionalization via the alcohol route

Complementary to the hydrothermal route, our group studied alcohol-based approaches to prepare nanostructures. Interestingly, a hybrid interface synergy is created by supercritical alcohols – used as reaction media – on the surface of ceria NPs [21, 22] in the absence of any organic surfactants. Through this approach, seven different alcohols were tested, namely MeOH, EtOH, PrOH, iPrOH, ButOH, PentOH, and HexOH. Their influence over the CeO_2 NC size, morphology, and surface properties in alcothermal conditions (T=300°C, p=24.5 MPa) was investigated. It was found that the CeO_2 size can be precisely tuned from 3 to 7 nm varying the alcohol length. However, the NPs were not dispersed but rather organized in spherical nanostructures of 20–100 nm (Figure 22B, C), exhibiting surfaces modified by alkoxide and carboxylate species, coming from the primary and secondary alcohol reaction with the ceria surface (Figure 22D, E). This study has demonstrated that the CeO_2 surface can be modified by using alcohols in near- or supercritical conditions acting both as solvents and surface stabilizers, thus avoiding the use of other surfactants. This method opened new synthesis pathways, giving the opportunity of using other solvents with an alcohol function, such as their amino derivatives [22].

Moving from oxide to pure metallic particles, Pd NCs were synthesized in supercritical acetone (T=250°C and p=20 MPa) [20, 39]. The main objective of this study was to control separately the nucleation/growth and the functionalization steps, by tuning the NCs' surface chemical functionalities and composition. Very reactive naked Pd NCs (up to 3 nm) were synthesized continuously in supercritical acetone, followed by their *ex situ* functionalization upon depressurization using perfluoro-1-decanethiol or 1-*n*-butyl-3-methylimidazolium hexafluorophosphate (ionic liquid) placed in the recovery vessel [39]. The presence of organic capped ligand on the surface of the Pd was monitored by coupling dynamic light scattering and nuclear magnetic resonance techniques, and catalytic

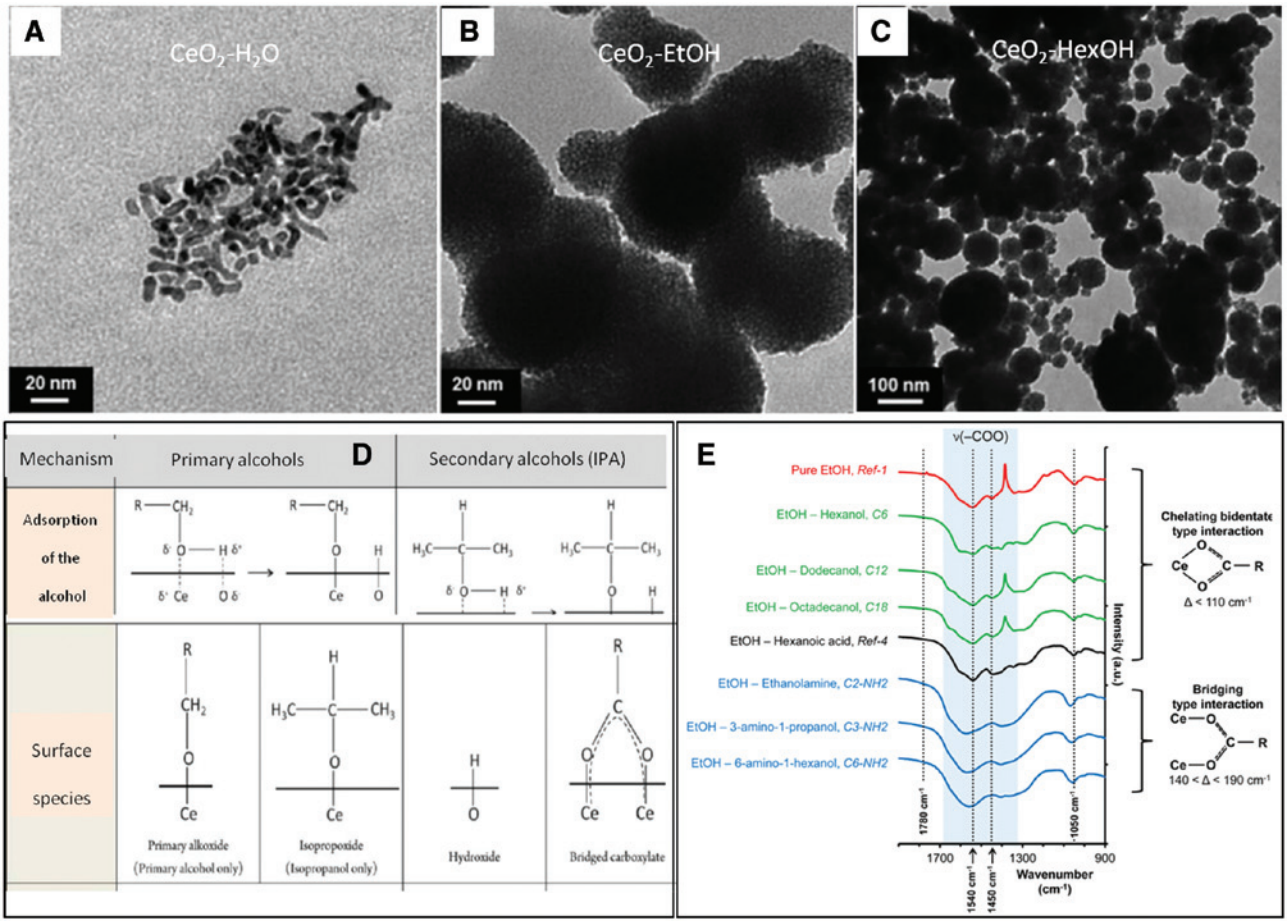

Figure 22: Ceria NPs prepared in supercritical alcohol and their derivatives, and ceria surface modification by the alcohol solvent. (A) Ceria NCs prepared in sc-H_2O as reference; (B) ceria prepared in sc-ethanol; and (C) ceria prepared in sc-hexanol. (D) Proposed mechanism of the surface reaction of primary and secondary alcohols with ceria. Reprinted with permission from Slostowski C, Marre S, Babot O, Toupance Th, Aymonier C, *Langmuir* 2012, 28, 16656–16663 [21], Copyright 2012 American Chemical Society. (E) FTIR and the surface species at the hybrid interface when supercritical alcohol derivatives are used for the ceria synthesis. Reprinted with permission from Slostowski C, Marre S, Babot O, Toupance Th, Aymonier C, *Langmuir* 2014, 30, 5965–5972 [22], Copyright 2014 American Chemical Society.

tests were successfully performed. For a better understanding of the process, Pd NCs were also recovered in a vessel in the absence of any organic stabilizer [20]. This alternative offered the possibility to incorporate non-metal atoms (C or H) at ambient conditions during the subsequent step to nucleation (step II B) and growth (step I) of palladium NCs in SCFs (Figure 23A). It was found that in the absence of any stabilizer, the primary Pd NCs keep growing by coalescence in the recovery vessel with the incorporation of other non-metal atoms (either already dissolved in the environment solution or coming from the ligand part of the precursor or the reaction solvent-acetone), and finally forming aggregates with different morphologies, depending on the considered precursor. It was demonstrated that Pd NCs chemistry (composition and surface energy) is influenced by the organic ligand of the Pd precursor but also by the reaction media. Although a layer of organic material was present at the surface of the Pd NC aggregates, it was possible to perform ligand exchange with thiols, thanks to their physisorbed nature allowing the redispersion of the Pd NCs in solution for further applications [20].

Synthesis of superparamagnetic ferrite NPs ($MnFe_2O_4$, Fe_3O_4) in supercritical ethanol (sc-EtOH) at a fairly moderate temperature (260°C) is yet another example of *in*(*ex*) *situ* functionalization [41]. The as-obtained NPs present good crystallinity, sizes <8 nm, monodispersity, superparamagnetic behavior at room temperature, and high saturation magnetization. Moreover, depending on the capping strategy, the ferrite NPs present extended (for *in situ* coated NPs) or short-term (for *ex situ* coated NPs) colloidal stability. Iron oxide NPs (~6 nm) were synthesized in the presence of an oleic acid/OAm mixture, comparable with the NPs obtained by thermal decomposition

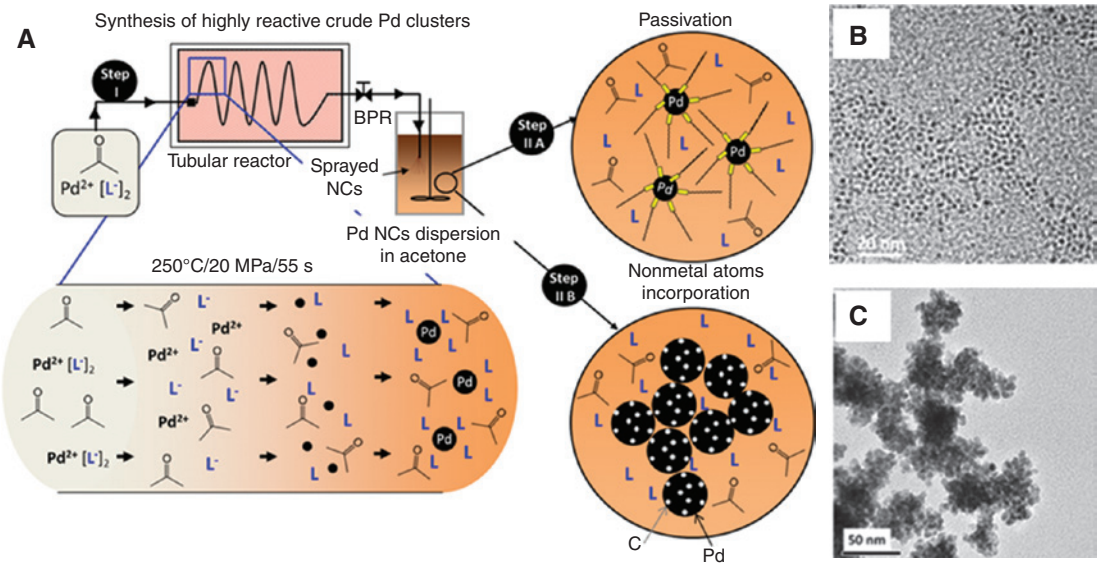

Figure 23: (A) Sketch of the continuous supercritical process for the synthesis of Pd NCs with separate control of the nucleation/growth and their subsequent surface modification. Reprinted with permission from Pascu O, Moisan S, Marty JD, Aymonier C, *J. Phys. Chem. C* 2014, 118, 14017–14025 [20], Copyright 2014 American Chemical Society. (B) TEM image of small thiol-capped Pd NCs and (C) naked Pd NCs forming aggregates in the absence of organic stabilizer.

(Figure 24). Moreover, the synthesis of $MnFe_2O_4$ with *in situ* functionalization afforded very small crystals (~2 nm), while the *ex situ* produced NPs of around 7 nm, underlying again the different behaviors for different metals in the same synthesis conditions.

The main limitation of the room temperature *ex situ* functionalization is the lower colloidal stability of the nanostructures. As the stabilizing agent is mainly physisorbed on the nano-objects' surface, its sorption/desorption occurs over time. Therefore, due to the higher reactivity of smaller NCs, growth through the Ostwald ripening mechanism was noticed. An optimized surface functionalization approach can be achieved by changing the continuous reactor type setup. The co-flow arrangement, developed by our group [40, 106–109], leading to the one-pot synthesis of multifunctional nanostructures, is a more versatile method detailed in the next paragraph.

2.2.3 Co-flow nanostructuration

To improve the process reproducibility and to achieve better control over nanostructures properties, it is advantageous to take the benefits of continuous synthetic methods

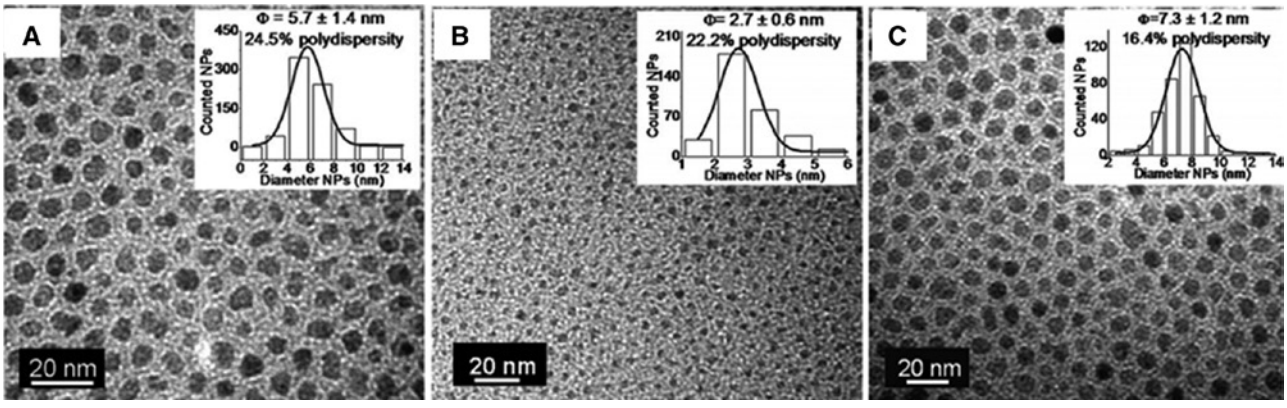

Figure 24: Superparamagentic ferrite NPs synthesized via supercritical ethanol route with *in*(*ex*) *situ* oleic acid (OAc) functionalization: (A) $FeFe_2O_4$@OAc NPs, (B) $MnFe_2O_4$@OAc NPs, and (C) $MnFe_2O_4$ naked NPs. Reprinted with permission from Pascu O, Marre S, Aymonier C, Roïg Y, *Nanoscale* 2013, 5, 2126–2132 [41], Copyright 2013 Royal Society of Chemistry.

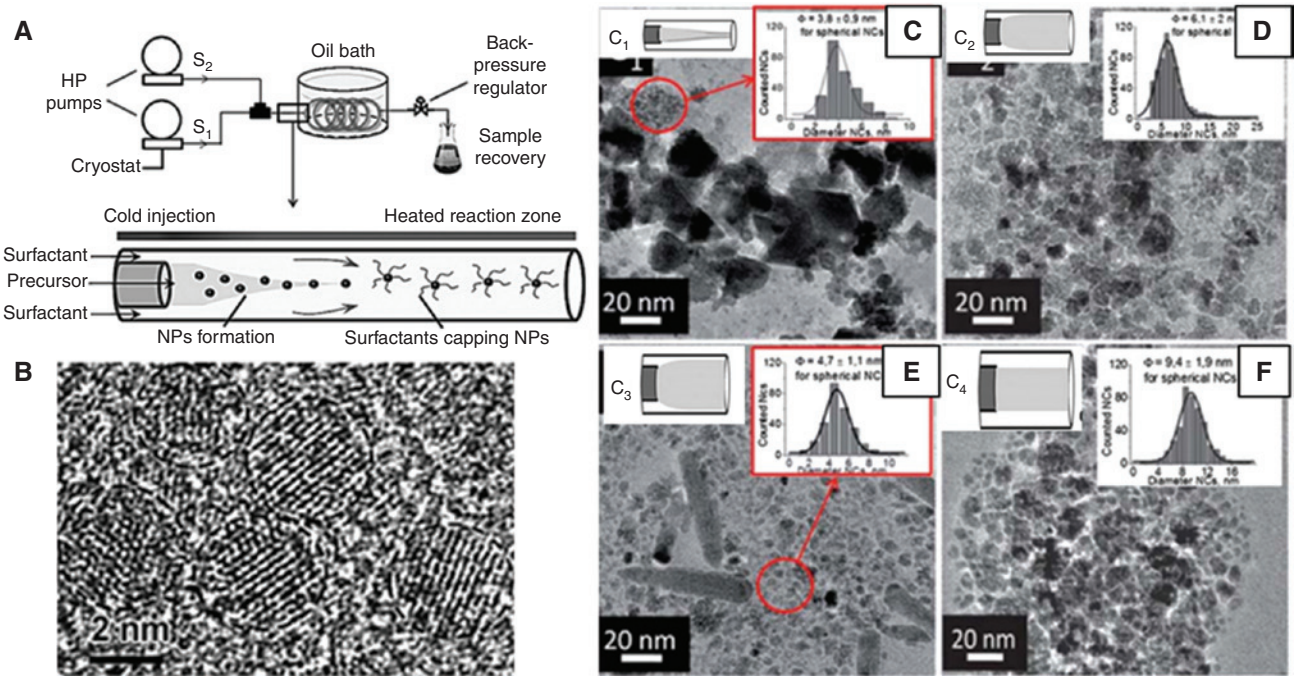

Figure 25: Micro- to milliscale co-flowing process for the synthesis of hybrid ZnO NCs. Reprinted with permission from Ilin ES, Marre S, Jubera V, Aymonier C, *J. Mater. Chem. C* 2013, 1, 5058–5063 [40], Copyright 2013 Royal Society of Chemistry, and from Roig Y, Marre S, Cardinal T, Aymonier C, Angew. Chem. Int. Ed. 2011, 50, 12071–12074 [106], Copyright 2011 Wiley.

based on milli-/microfluidics. A separate control of nucleation/growth and functionalization steps can be performed in a hydrodynamically controlled environment provided by microscale reactors. In particular, we have developed a co-axial flowing microsystem made of two fused silica capillaries inserted in one another with inner diameters of hundreds of micrometers and a specific length, adapted for each experiment. Heating was provided by an oil bath, whereas the pressure was controlled with a back-pressure regulator downstream (p=25 MPa). The precursor solution (~10^{-2} M) is injected in the inner capillary and the second solution, containing the capping agent, is externally injected (Figure 25A) [40, 106]. The co-axial injection ensures a 3D positioning of the precursor flow at the center of the main tubing, allowing an easily interchanging of capping ligands without influencing the NC core size or structure. The first material prepared with this setup was ZnO NCs [106], whose size around 4 nm was independent from the considered organic ligand (OAm, TOP, or oleic acid), in agreement with the separation of the nucleation/growth and functionalization steps (Figure 25B). At the microscale co-flowing synthesis processes, the importance of hydrodynamics is crucial, clearly visible in NC size and properties by variation of the velocities ratio of the internal to external flow (R_H). A flow-focusing regime appears when the ratio is <1 and a flow-spreading one for R_H>1, influencing the interaction between nucleation/growth and NC functionalization processes [40]. Because of the small quantity of produced materials using microreactors, an important work was done to investigate the influence of the scale-up effect from continuous microfluidic up to millifluidic systems over the synthesized ZnO NCs' optical properties [40]. Different hydrodynamic regimes, as a consequence of different reactors' configurations, show great influence over the ZnO NCs morphology (Figure 25C–F), although the nanomaterials' enhanced optical properties were kept constant [40].

Similarly, an adapted co-flowing setup was further used to synthesize hybrid Pd nanocatalysts [107, 108]. The main interest was to evaluate the influence of the stereoelectronic properties of the capping ligand over the catalysis efficiency independently from the Pd core characteristics. A variety of nanocatalysts displaying different electronic and steric properties were synthesized, such as Pd@dppf and Pd@PCy_3, where dppf and PCy_3 stand for 1,1′-bis(diphenylphosphino)ferrocene and tri(cyclohexyl) phosphane, respectively, [108]. Pd@dppf NCs (~2.4 nm) were monodispersed, almost spherical, with a narrow size distribution and a very good crystallinity in contrast to the larger and aggregated Pd@PCy_3 NCs. The difference was attributed to the type of ligand, with dppf being more bulky, thus it can better shield the formed nuclei,

therefore impeding a further growth. Over time, owing to their high reactivity, Ostwald ripening occurs and larger NPs are formed but at the expense of losing catalytic activity. The Pd@PCy_3 system behaves completely differently; the already aggregated NCs are stable over time, keeping the same catalytic activity.

The versatility of the co-flow approach was later demonstrated with the synthesis at high temperature and high pressure of cerium-based metal-organic framework exhibiting the same phase as microparticles obtained under conventional batch solvothermal conditions but in exceptionally much shorter residence times (30 s) compared to the 12 h reaction time required for the classical batch approach, opening avenues toward production scale-up [109].

3 Conclusion

SCF processes (SFCD and CSFS) have already been demonstrated to be very useful approaches for creating interfaces at nanoscale. This capability has been used to synthesize nano building blocks with controlled characteristics, as well as to design nanostructured advanced materials (inorganic or hybrid), combining multiple materials and functionalities. These were successfully implemented in various applications including catalysis, optics, electronics, etc.

While the environmental interest in SCFs such as sc-CO_2 or sc-water (highlighted in this review) brings opportunities for the sustainable design of materials, it is their unique physico-chemical properties that have – and will – drive their use in materials synthesis. Indeed, being able to perform liquid-phase synthesis in a gas-like environment displaying a quasi-zero surface tension is particularly favorable to promote an effective nanostructuration of complicated architectures and confined geometries.

These processes are therefore a good example of technology that can address the current challenges of materials science, while being able to adapt itself to the societal demands. Indeed, SCF processes are not anymore a laboratory curiosity, as several industrial SCF synthesis plants are now operated worldwide.

References

[1] Sanchez C, Boissiere C, Cassaignon S, Chaneac C, Durupthy O, Faustini M, Grosso D, Laberty-Robert C, Nicole L, Portehault D, Ribot F, Rozes L, Sassoye C. Molecular engineering of functional inorganic and hybrid materials. *Chem. Mater.* 2014, 26, 221–238.

[2] Mehdi A, Reye C, Corriu R. From molecular chemistry to hybrid nanomaterials: design and functionalization. *Chem. Soc. Rev.* 2011, 40, 563–574.

[3] Cansell F, Aymonier C. Design of functional nanostructured materials using supercritical fluids. *J. Supercritical Fluids* 2009, 47, 508–516.

[4] Yuan J, Müller AHE. One-dimensional organic-inorganic hybrid nanomaterials. *Polymer* 2010, 51, 4015–4036.

[5] Willner I, Willner B. Biomolecule-based nanomaterials and nanostructures. *Nano Lett.* 2010, 10, 3805–3815.

[6] Mendes PM. Cellular nanotechnology: making biological interfaces smarter. *Chem. Soc. Rev.* 2013, 42, 9207–9218.

[7] Ding M, Tang Y, Star A. Understanding interfaces in metal-graphitic hybrid nanostructures. *J. Phys. Chem. Lett.* 2013, 4, 147–160.

[8] Motornov M, Roiter Y, Tokarev I, Minko S. Stimuli-responsive nanoparticles, nanogels and capsules for integrated multifunctional intelligent systems. *Progress Pol. Sci.* 2010, 35, 174–211.

[9] Rawolle M, Niedermeier MA, Kaune G, Perlich J, Lellig Ph, Memesa M, Cheng Y-J, Gutmann JS, Muller-Buschbaum P. Fabrication and characterization of nanostructured titania films with integrated function from inorganic-organic hybrid materials. *Chem. Soc. Rev.* 2012, 41, 5131–5142.

[10] Liang Y, Li Y, Wang H, Da H. Strongly coupled inorganic/nanocarbon hybrid materials for advanced electrocatalysis. *J. Am. Chem. Soc.* 2013, 135, 2013–2036.

[11] Yu G, Xie X, Pan L, Bao Zh, Cui Y. Hybrid nanostructured materials for high-performance electrochemical capacitors. *Nano Energy* 2013, 2, 213–234.

[12] Mohana Reddy AL, Gowda SR, Shaijumon MM, Ajayan PM. Hybrid nanostructures for energy storage applications. *Adv. Mater.* 2012, 24, 5045–5064.

[13] Lee J-H, Singer JP, Thomas EL. Micro-/nanostructured mechanical metamaterials. *Adv. Mater.* 2012, 24, 4782–4810.

[14] Layani M, Kamyshny A, Magdassi S. Transparent conductors composed of nanomaterials. *Nanoscale* 2014, 6, 5581–5591.

[15] Li S-S, Chen C-W. Polymer-metal-oxide hybrid solar cells. *J. Mater. Chem. A* 2013, 1, 10574–10591.

[16] Lee S-Y, Lim J-S, Harris MT. Synthesis and application of virus-based hybrid nanomaterials. *Biotech. Bioeng.* 2012, 109, 16–30.

[17] Fattahi P, Yang G, Kim G, Abidian MR. A review of organic and inorganic biomaterials for neural interfaces. *Adv. Mater.* 2014, 26, 1846–1885.

[18] Pascu O, Cacciuttolo B, Marre S, Pucheault M, Aymonier C. $ScCO_2$ assisted preparation of supported metal NPs: application to catalyst design. *J. Supercritical Fluids*, 2015. DOI: 10.1016/j.supflu.2014.11.013.

[19] Aymonier C, Denis A, Roig Y, Iturbe M, Sellier E, Marre S, Cansel F, Bobet JL. Supported metal NPs on magnesium using SCFs for hydrogen storage: interface and interphase characterization. *J. Supercrit. Fluids* 2010, 53, 102–107.

[20] Pascu O, Moisan S, Marty J-D, Aymonier C. Highly reactive Pd NCs by versatile continuous supercritical fluids synthesis for the preparation of metal-nonmetal Pd-based NCs. *J. Phys. Chem. C* 2014, 118, 14017–14025.

[21] Slostowski C, Marre S, Babot O, Toupance TH, Aymonier C. Near- and supercritical alcohols as solvents and surface modifiers for the continuous synthesis of cerium oxide nanoparticles. *Langmuir* 2012, 28, 16656–16663.

[22] Slostowski C, Marre S, Babot O, Toupance Th, Aymonier C. CeO_2 nanocrystals from supercritical alcohols: new opportunities for versatile functionalizations? *Langmuir* 2014, 30, 5965–5972.
[23] Bozbag SE, Erkey C. Supercritical deposition: current status and perspectives for the preparation of supported metal nanostructures. *J. Supercrit. Fluid* 2015, 96, 298–312.
[24] Sanli D, Bozbag SE, Erkey C. Synthesis of nanostructured materials using supercritical CO_2: Part I. Physical transformations. *J. Mater. Sci.* 2012, 47, 2995–3025.
[25] Bozbag SE, Sanli D, Erkey C. Synthesis of nanostructured materials using supercritical CO_2: Part II. Chemical transformations. *J. Mater. Sci.* 2012, 47, 3469–3492.
[26] Philippot G, Elissalde C, Maglione M, Aymonier C. Supercritical fluid technology: a reliable process for high quality $BaTiO_3$ based nanomaterials. *Adv. Powder Technol.* 2014, 25, 1415–1429.
[27] Aymonier C, Loppinet-Serani A, Reveron H, Garrabos Y, Cansell F. Review of supercritical fluids in inorganic materials science. *J. Supercrit. Fluid* 2006, 38, 242–251.
[28] Sui R, Charpentier P. Synthesis of metal oxide nanostructures by direct sol–gel chemistry in supercritical fluids. *Chem. Rev.* 2012, 112, 3057–3082.
[29] Pinho B, Girardon S, Ba-Bachi F, Bergeot G, Marre S, Aymonier C. A microfluidic approach for investigating multicomponent system thermodynamics at high pressures and temperatures. *Lab Chip* 2014, 14, 3843–3849.
[30] Pinho B, Girardon S, Bazer-Bachi F, Bergeot G, Marre S, Aymonier C. Simultaneous measurements of fluids density and viscosity using HP/HT capillary devices. *J. Supercrit. Fluid*, 2015. DOI: SUPFLU-D-14-00376R1.
[31] Majimel M, Marre S, Garrido E, Aymonier C. Supercritical fluid chemical deposition as an alternative process to CVD for the surface modification of materials. *Chem. Vap. Depos.* 2011, 17, 342–352.
[32] Marre S, Cansell F, Aymonier C. Design at the nanometre scale of multifunctional materials using supercritical fluid chemical deposition. *Nanotechnology* 2006, 17, 4594–4599.
[33] Watkins JJ, Blackburn JM, McCarthy TJ. Chemical fluid deposition: reactive deposition of platinum metal from carbon dioxide solution. *Chem. Mater.* 1999, 11, 213–215.
[34] Blackburn JM, Long DP, Cabañas A, Watkins JJ. Deposition of conformal copper and nickel films from supercritical carbon dioxide. *Science* 2001, 294, 141–145.
[35] Zhang Y, Erkey C. Preparation of supported metallic nanoparticles using supercritical fluids: a review. *J. Supercrit. Fluid* 2006, 38, 252–267.
[36] Erkey C. Preparation of metallic supported nanoparticles and films using supercritical fluid deposition. *J. Supercrit. Fluid* 2009, 47, 517–522.
[37] Marre S, Erriguible A, Perdomo A, Cansell F, Marias F, Aymonier C. Kinetically controlled formation of supported nanoparticles in low temperature supercritical media for the development of advanced nanostructured materials. *J. Phys. Chem. C* 2009, 113, 5096–5104.
[38] Adshiri T. Supercritical hydrothermal synthesis of organic-inorganic hybrid nanoparticles. *Chem. Lett.* 2007, 36, 1188–1193.
[39] Moisan S, Marty J-D, Cansell F, Aymonier C. Preparation of functional hybrid palladium nanoparticles using supercritical fluids: a novel approach to detach the growth and functionalization steps. *Chem. Commun.* 2008, 1428–1430.
[40] Ilin ES, Marre S, Jubera V, Aymonier C. Continuous supercritical synthesis of high quality UV-emitting ZnO nanocrystals for optochemical applications. *J. Mater. Chem. C* 2013, 1, 5058–5063.
[41] Pascu O, Marre S, Aymonier C, Roig A. Ultrafast and continuous synthesis of crystalline ferrite nanoparticles in supercritical ethanol. *Nanoscale* 2013, 5, 2126–2132.
[42] Cabanas A, Blackburn JM, Watkins JJ. Deposition of Cu films from supercritical fluids using Cu(I)b-diketonate precursors. *Microelectr. Eng.* 2002, 64, 53–61.
[43] Zong Y, Watkins JJ. Deposition of Copper by the H_2-assisted reduction of $Cu(tmod)_2$ in supercritical carbon dioxide: kinetics and reaction mechanism. *Chem. Mater.* 2005, 17, 560–565.
[44] Cabañas A, Long DP, Watkins JJ. Deposition of gold films and nanostructures from supercritical carbon dioxide. *Chem. Mater.* 2004, 16, 2028–2033.
[45] Karanikas ChF, Watkins JJ. Kinetics of the ruthenium thin film deposition from supercritical carbon dioxide by the hydrogen reduction of $Ru(tmhd)_2cod$. *Microelectr. Eng.* 2010, 87, 566–572.
[46] Boyd EP, Ketchum DR, Deng H, Shore SG. Chemical vapor deposition of metallic thin films using homonuclear and heteronuclear metal carbonyls. *Chem. Mater.* 1997, 9, 1154–1158.
[47] Krisyuka VV, Shubina YV, Senocq F, Turgambaeva AE, Duguet T, Igumenoa IK, Vahlas C. Chemical vapor deposition of Pd/Cu alloy films from a new single source precursor. *J. Cryst. Growth* 2015, 414, 130–134.
[48] Cheng F, George K, Hector AL, Jura M, Kroner A, Levason W, Nesbitt J, Reid G, Smith DC, Wils JW. Chemical vapor deposition of GaP and GaAs thin films from [nBu2Ga(μ-EtBu2)2GanBu2] (E=P or As) and Ga(PtBu2)3. *Chem. Mater.* 2011, 23, 5217–5222.
[49] O'Neil A, Watkins JJ. Reactive deposition of conformal metal oxide films from supercritical carbon dioxide. *Chem. Mater.* 2007, 19, 5460–5466.
[50] Mesguich D, Aymonier C, Bassat J-M, Mauvy F, You E, Watkins JJ. Low-temperature deposition of undoped ceria thin films in sc-CO_2 as improved interlayers for IT-SOFC. *Chem. Mater.* 2011, 23, 5323–5330.
[51] Watkins JJ, McCarthy TJ. Polymer/metal nanocomposite synthesis in supercritical CO_2. *Chem. Mater.* 1995, 7, 1991–1994.
[52] Müller S, Türk M. Production of supported gold and gold-silver nanoparticles by supercritical fluid reactive deposition: effect of substrate properties. *J. Supercrit. Fluid* 2015, 96, 287–297.
[53] Aschenbrenner O, Kemper S, Dahmen N, Schaber K, Dinjus E. Solubility of β-diketonates, cyclopentadienyls, and cyclooctadiene complexes with various metals in supercritical carbon dioxide. *J. Supercrit. Fluid* 2007, 41, 179–186.
[54] Morère J, Tenorio MJ, Pando C, Renuncio JAR, Cabañas A. Solubility of two metal-organic ruthenium precursors in supercritical CO_2 and their application in supercritical fluid technology. *J. Chem. Thermodyn.* 2013, 58, 55–61.
[55] Tenorio MJ, Cabañas A, Pando C, Renuncio JAR. Solubility of Pd(hfac)2 and Ni(hfac)2·2H_2O in supercritical carbon dioxide pure and modified with ethanol. *J. Supercrit. Fluid* 2012, 70, 106–111.
[56] Tenorio MJ, Pando C, Renuncio JAR, Stevens JG, Bourne RA, Poliakoff M, Cabañas A. Adsorption of $Pd(hfac)_2$ on mesoporous silica SBA-15 using supercritical CO_2 and its role in the performance of Pd-SiO_2 catalyst. *J. Supercrit. Fluid* 2012, 69, 21–28.

[57] Zhang Y, Cangul B, Garrabos Y, Erkey C. Thermodynamics and kinetics of adsorption of bis(2,2,6,6-tetramethyl-3,5-heptanedionato) (1,5-cyclooctadiene) ruthenium (II) on carbon aerogel from supercritical CO_2 solution. *J. Supercrit. Fluid* 2008, 44, 71–77.
[58] Türk M. Influence of thermodynamic behavior and solute properties on homogeneous nucleation in supercritical solutions. *J. Supercrit. Fluid* 2000, 18, 169–184.
[59] Garrido GI, Patcas FC, Upper G, Türk M, Yilmaz S, Kraushaar-Czarnetzki B. Supercritical deposition of Pt on SnO_2-coated Al_2O_3 foams: phase behaviour and catalytic performance. *Appl. Catal. A Gen.* 2008, 338, 58–65.
[60] Lang S, Türk M, Kraushaar-Czarnetzki B. Novel PtCuO/CeO2/a-Al_2O_3 sponge catalysts for the preferential oxidation of CO (PROX) prepared by means of supercritical fluid reactive deposition (SFRD). *J. Catal.* 2012, 286, 78–87.
[61] Bozbag SE, Unal U, Kurykin MA, Ayala CJ, Aindow M, Erkey C. Thermodynamic control of metal loading and composition of carbon aerogel supported Pt-Cu alloy nanoparticles by supercritical deposition. *J. Phys. Chem. C* 2013, 117, 6777–6787.
[62] Zhang Y, Kang D, Aindow M, Erkey C. Preparation and characterization of ruthenium/carbon aerogel nanocomposites via a supercritical fluid route. *J. Phys. Chem. B* 2005, 109, 2617–2624.
[63] Cangül B, Zhang LC, Aindow M, Erkey C. Preparation of carbon black supported Pd, Pt and Pd-Pt nanoparticles using supercritical CO_2 deposition. *J. Supercrit. Fluid* 2009, 50, 82–90.
[64] Bayrakceken A, Cangul B, Zhan LC, Aindow M, Erkey C. PtPd/BP2000 electrocatalysts prepared by sequential supercritical carbon dioxide deposition. *Int. J. Hydr. Energ.* 2010, 35, 11669–11680.
[65] Zhao J, Yu H, Liu Z, Ji M, Zhang L, Sun G. Supercritical deposition route of preparing Pt/graphene composites and their catalytic performance toward methanol electrooxidation. *J. Phys. Chem. C* 2014, 118, 1182–1190.
[66] Zhao J, Zhang L, Xue H, Wang Z, Hu H. Methanol electrocatalytic oxidation on highly dispersed platinum-ruthenium/ graphene catalysts prepared in supercritical carbon dioxide-methanol solution. *RSC Adv.* 2012, 2, 9651–9659.
[67] Bayrakceken A, Kitkamthorn U, Aindow M, Erkey C. Decoration of multi-wall carbon nanotubes with platinum nanoparticles using supercritical deposition with thermodynamic control of metal loading. *Script. Mater.* 2007, 56, 101–103.
[68] Xu Q-Q, Zhang C-J, Zhang X-Z, Yin J-Z, Liu Y. Controlled synthesis of Ag nanowires and nanoparticles in mesoporous silica using supercritical carbon dioxide and co-solvent. *J. Supercrit. Fluid* 2012, 62, 184–189.
[69] Zhang Y, Kang D, Saquing C, Aindow M, Erkey C. Supported platinum nanoparticles by supercritical deposition. *Ind. Eng. Chem. Res.* 2005, 44, 4161–4164.
[70] Saquing CD, Kang D, Aindow M, Erkey C. Investigation of the supercritical deposition of platinum nanoparticles into carbon aerogels. *Micropor. Mesopor. Mater.* 2005, 80, 11–23.
[71] Daly B, Arnold DC, Kulkarni JS, Kazakova O, Shaw MT, Nikitenko S, Erts D, Morris MA, Holmes JD. Synthesis and characterization of highly ordered cobalt-magnetite nanocable arrays. *Small* 2006, 2, 1299–1307.
[72] Aggarwal V, Reichenbach LF, Enders M, Muller T, Wolff S, Crone M, Türk M, Bräse S. Influence of perfluorinated end groups on the SFRD of [Pt(cod)Me(CnF_{2n+1})] onto porous Al_2O_3 in CO_2 under reductive conditions. *Chem. Eur. J.* 2013, 19, 12794–12799.
[73] Pelka J, Gehrke H, Esselen M, Türk M, Crone M, Bräse S, Muller T, Blank H, Send W, Zibat V, Brenner P, Schneider R, Gerthsen D, Marko D. Cellular uptake of platinum nanoparticles in human colon carcinoma cells and their impact on cellular redox systems and DNA integrity. *Chem. Res. Toxicol.* 2009, 22, 649–659.
[74] Wong B, Yoda S, Howdle SM. The preparation of gold nanoparticle composites using supercritical carbon dioxide. *J. Supercrit. Fluid* 2007, 42, 282–287.
[75] Erriguible A, Marias F, Cansell F, Aymonier C. Monodisperse model to predict the growth of inorganic nanostructured particles in supercritical fluids through a coalescence and aggregation mechanism. *J. Supercrit. Fluid* 2009, 48, 79–84.
[76] Couillaud S, Kirikova M, Zaïdi W, Bonnet J-P, Marre S, Aymonier C, Zhang J, Cuevas F, Latroche M, Aymard L, Bobet J-L. Supercritical fluid chemical deposition of Pd nanoparticles on magnesium-scandium alloy for hydrogen storage. *J. Alloys Comp.* 2013, 574, 6–12.
[77] Bobet JL, Aymonier C, Desguich D, Cansell F, Asano K, Akiba E. Particles decoration in supercritical fluid to improve the hydrogen sorption cyclability of magnesium, *J. Alloys Compd.* 2007, 429, 250–254.
[78] Rezayat M, Blundell RK, Camp JE, Walsh DA, Thielemans W. Green one-step synthesis of catalytically active palladium nanoparticles supported on cellulose nanocrystals. *ACS Sustain. Chem. Eng.* 2014, 2, 1241–1250.
[79] Rangappa D, Sone K, Zhou Y, Kud T, Honma I. Size and shape controlled $LiMnPO_4$ nanocrystals by supercritical ethanol process and their electrochemical properties. *J. Mater. Chem.* 2011, 21, 15813–15818.
[80] Davidson FM III, Schrinker AD, Wiacek RJ, Korgel BA. Supercritical fluid-liquid-solid synthesis of gallium arsenide nanowires seeded by alkanethiol-stabilized gold nanocrystals. *Adv. Mater.* 2004, 16, 646–649.
[81] Barrett ChA, Gunning RD, Hantschel Th, Arstila K, O'Sullivan C, Geaney H, Ryan KM. Metal surface nucleated supercritical fluid-solid-solid growth of Si and Ge/SiO_x core-shell nanowires, *J. Mater. Chem.* 2010, 20, 135–144.
[82] Moisan S, Martinez V, Weisbecker P, Cansell F, Mecking S, Aymonier C. General approach for the synthesis of organic-inorganic hybrid nanoparticles mediated by supercritical CO_2. *J. Am Chm. Soc.* 2007, 129, 10602–10606.
[83] Cimpeanu V, Kocevar M, Parvulescu VI, Leitner W. Preparation of rhodium nanoparticles in carbon dioxide induced ionic liquids and their application to selective hydrogenation. *Angew. Chem. Int. Ed.* 2009, 48, 1085–1088.
[84] Pascu O, Liautard V, Vaultier M, Pucheault M, Aymonier C. Catalysed stereodivergent hydrosilylation with onium salts stabilised M(0) nanocatalysts prepared in $scCO_2$. *RSC Adv.* 2014, 4, 59953–59960.
[85] Liautard V, Pascu O, Aymonier C, Pucheault M. Advanced nanostructured catalysts for hydroboration. *Catal. Today* 2015, 255, 60–65.
[86] Adschiri T, Lee Y-W, Goto M, Takami S. Green materials synthesis with supercritical water. *Green Chem.* 2011, 13, 1380–1390.
[87] Atashfaraza M, Shariaty-Niassar M, Ohara S, Minami K, Umetsua M, Naka T, Adschiri T. Effect of titanium dioxide solubility on the formation of $BaTiO_3$ nanoparticles in supercritical water. *Fluid Phase Equilibr.* 2007, 257, 233–237.
[88] Philippo G, Jensen KMØ, Christensen M, Elissalde C, Maglione M, Iversen BB, Aymonier C. Coupling in situ synchrotron

radiation with ex situ spectroscopy characterizations to study the formation of $Ba_{1-x}Sr_xTiO_3$ nanoparticles in supercritical fluids *J. Supercrit. Fluid* 2014, 87, 111–117.
[89] Reveron H, Aymonier C, Loppinet-Serani A, Elissalde C, Maglione M, Cansell F. Single-step synthesis of well-crystallized and pure barium titanate nanoparticles in supercritical fluids. *Nanotechnology* 2005, 16, 1137–1143.
[90] Sue K, Kakinuma N, Adschiri T, Arai K. Continuous production of nickel fine particles by hydrogen reduction in near-critical water. *Ind. Eng. Chem. Res.* 2004, 43, 2073–2078.
[91] Desmoulins-Krawiec S, Aymonier C, Loppinet-Serani A, Weill F, Gorsse S, Etourneau J, Cansell F. Synthesis of nanostructured materials in supercritical ammonia: nitrides, metals and oxides. *J. Mater. Chem*. 2004, 14, 228–232.
[92] Byrappa K, Adschiri T. Hydrothermal technology for nanotechnology. *Progr. Cryst. Growth Char. Mater.* 2007, 53, 117–166.
[93] Byrappa K, Ohara S, Adschiri T. Nanoparticles synthesis using supercritical fluid technology – towards biomedical applications. *Adv. Drug Deliv. Rev.* 2008, 60, 299–327.
[94] Zhang J, Ohara S, Umetsu M, Naka T, Hatakeyama Y, Adschiri T. Colloidal ceria nanocrystals: a tailor-made crystal morphology in supercritical water. *Adv. Mater.* 2007, 19, 203–206.
[95] Kaneko K, Inoke K, Freitag B, Hungria AB, Midgley PA, Hansen ThW, Zhang J, Ohara S, Adschiri T. Structural and morphological characterization of cerium oxide nanocrystals prepared by hydrothermal synthesis. *Nano Lett.* 2007, 7, 421–425.
[96] Takami S, Ohara S, Adschiri T, Wakayama Y, Chikyow T. Continuous synthesis of organic–inorganic hybridized cubic nanoassemblies of octahedral cerium oxide nanocrystals and hexanedioic acid. *Dalton Trans.* 2008, 5442–5446.
[97] Taguchi M, Yamamoto N, Hojo D, Takami S, Adschiri T, Funazukuri T, Naka T. Synthesis of monocarboxylic acid-modified CeO_2 nanoparticles using supercritical water. *RSC Adv.* 2014, 4, 49605–49613.
[98] Sahraneshin A, Asahina S, Togashi T, Singh V, Takami S, Hojo D, Arita T, Minami K, Adschiri T. Surfactant-assisted hydrothermal synthesis of water-dispersible hafnium oxide nanoparticles in highly alkaline media. *Cryst. Growth Des*. 2012, 12, 5219–5226.
[99] Togashi T, Naka T, Asahina S, Sato K, Takami S, Adschiri T. Surfactant-assisted one-pot synthesis of superparamagnetic magnetite nanoparticle clusters with tunable cluster size and magnetic field sensitivity. *Dalton Trans.* 2011, 40, 1073–1078.
[100] Togashi T, Takami S, Kawakami K, Yamamoto H, Naka T, Sato K, Abeand K, Adschiri T. Continuous hydrothermal synthesis of 3,4 dihydroxyhydrocinnamic acid-modified magnetite nanoparticles with stealth-functionality against immunological response. *J. Mater. Chem.* 2012, 22, 9041–9045.
[101] Ohara S, Mousavand T, Sasaki T, Umetsu M, Naka T, Adschiri T. Continuous production of fine zinc oxide nanorods by hydrothermal synthesis in supercritical water. *J. Mater. Sci.* 2008, 43, 2393–2396.
[102] Mousavand T, Ohara S, Naka T, Umetsu M, Takami S, Adschiri T. Organic-ligand-assisted hydrothermal synthesis of ultrafine and hydrophobic ZnO nanoparticles. *J. Mater. Res.* 2010, 25, 219–223.
[103] Daschner de Tercero M, Röder C, Fehrenbacher U, Teipel U, Türk M. Continuous supercritical hydrothermal synthesis of iron oxide nanoparticles dispersion and their characterization. *J. Nanopart. Res.* 2014, 16, 2350-1–2350-27.
[104] Daschner de Tercero M, Gonzales Martinez I, Herrmann M, Bruns M, Kübel Ch, Jennewein S, Fehrenbacher U, Barner L, Türk M. Synthesis of *in situ* functionalized iron oxide nanoparticles presenting alkyne groups via a continuous process using near-critical and supercritical water. *J. Supercrit. Fluid* 2013, 82, 83–95.
[105] Daschner de Tercero M, Bruns M, Gonzales Martinez I, Türk M, Fehrenbacher U, Jennewein S, Barner L. Continuous hydrothermal synthesis of *in situ* functionalized iron oxide nanoparticles – a general strategy to produce metal oxide nanoparticles presenting clickable anchors. *Part. Part. Syst. Charact.* 2013, 30, 229–234.
[106] Roig Y, Marre S, Cardinal T, Aymonier C. Synthesis of exciton luminescent ZnO nanocrystals using continuous supercritical microfluidics. *Angew. Chem. Int. Ed.* 2011, 50, 12071–12074.
[107] Gendrineau T, Marre S, Vaultier M, Pucheault M, Aymonier C. Microfluidic synthesis of palladium nanocrystals assisted by supercritical CO_2: tailored surface properties for applications in boron chemistry. *Angew. Chem. Int. Ed.* 2012, 51, 1–5.
[108] Pascu O, Marciasini L, Marre S, Vaultier M, Pucheault M, Aymonier C. Continuous coflow synthesis of hybrid palladium nanocrystals as catalysts for borylation reaction. *Nanoscale* 2013, 5, 12425–12431.
[109] D'Arras L, Sassoye C, Rozes L, Sanchez C, Marrot J, Marre S, Aymonier C. Fast and continuous processing of a new submicronic lanthanide-based metal-organic framework. *New J. Chem.* 2014, 38, 1477–1483.